NZE 25-(EQC 1991/38)

Analysis of the Weber (Dannevirke) Earthquakes of 2 February and 13 May 1990, and their Aftershocks

R Robinson, IGNS

Final Report, Research Project 91/38, "Analysis of the Weber (Dannevirke) Earthquakes of 2 February and 13 May 1990, and their Aftershocks"

Russell Robinson

Institute of
GEOLOGICAL & NUCLEAR SCIENCES
Limited

Contract Report No. 1992/64

Institute of
GEOLOGICAL
& NUCLEAR
SCIENCES
Limited

FINAL REPORT, RESEARCH PROJECT 91/38, "ANALYSIS OF THE WEBER (DANNEVIRKE) EARTHQUAKES OF 2 FEBRUARY AND 13 MAY 1990, AND THEIR AFTERSHOCKS"

CONTRACT REPORT NO. 1992/64

Prepared for:

Earthquake & War Damage Commission

Russell Robinson
Seismological Observatory
Institute of Geological and Nuclear Sciences
(Formerly DSIR Geology & Geophysics)

August 1992

32 Salamanca Road, PO Box 1320, Wellington, New Zealand, Telephone: +64-4-473 8208, Facsimile: +64-4-471 0977

A Crown Research Institute

Final Report, Research Project 91/38, "Analysis of the Weber (Dannevirke) Earthquakes of 2 February and 13 May 1990, and their Aftershocks"

Russell Robinson

This project has been completed up to the stage of a research paper, intended for submission to the Bulletin of the Seismological Society of America. A copy of this paper is enclosed as the major part of this final report. A lecture based on this work was given at the June meeting of the Geophysics Section, Royal Society of New Zealand.

As indicated by the title of the paper, the occurrence of further large events near Weber in August 1990 and March 1992, meant that the scope of the study has necessarily been widened from the original proposal. This also caused the project to be somewhat behind schedule. Still, the research work is now complete. Many of the computer programs written for this work can now be applied to the study of future large events, making that task much easier and quicker.

I would like to thank the Commission for making this research possible, and I hope that the results are satisfactory.

SUMMARY OF RESULTS

Velocity Model and Its Implications:

Digital data for earthquakes in the Weber region have been used to derive a seismic velocity model for the region, and also to obtain magnitude corrections. The velocity model, which is one-dimensional but includes station terms, indicates that: 1) Low-velocity Cenozoic sediments thicken to the east and north; 2) Underlying these sediments, the crust of the Australian plate is similar to that near Wellington, i.e. probably it consists of greywacke grading downward to schist; 3) At the interface between the Australian and Pacific plates (19 km depth) there is a low-velocity layer, probably reflecting the subduction of some thickness of low velocity sediments; 4) The seismic velocity deeper in the subducted plate is very high, 8.8 km/sec or more.

Fault Geometry:

The velocity model has been used to relocate 4151 earthquakes, mostly aftershocks, in the Weber region. The locations have been graded as to quality. The very best hypocentres have been used to examine the geometry of the two faults involved in the largest mainshocks. The first event, February 19, 1990, occurred on a NE striking and steeply dipping (75 degrees NW) fault within the subducted Pacific plate, extending from 23 to 33 km depth. The second event, May 13, 1990, occurred on a NE striking and shallowly dipping (35 degrees NW) imbricate fault in the overlying Australian plate, 7 to 18 km deep. It was NOT on the plate interface as originally thought. There seems to be some curvature to the fault plane.

Focal Mechanisms and Tectonic Implications:

Focal mechanisms have been obtained for the two largest events and many of their aftershocks, using data from portable seismographs installed in the epicentral regions. The mainshock in February involved normal dip-slip motion, reflecting the down-dip tension due to "slab pull" within the subducted Pacific plate. This is a larger example of the faulting that is common throughout the subducted plate along the east coast of the North Island. The mainshock in May involved primarily thrust faulting but with a component of dextral strike-slip. Although the fault plane is oriented NE-SW, oblique to the direction of plate convergence, the slip vector is oriented close to the convergence direction. Aftershocks of both events had a wide variety of mechanisms, but on average were similar to the main shocks.

Although the tectonic situation would predict the occurrence of shallow-dipping thrust events along the plate interface, there is little evidence for such events in New Zealand. It may be that the thicker and more buoyant nature of the subducting crust now makes these events more rare than in the past, the plate convergence being taken up as in a continent-continent type collision zone. This idea is supported by the fact that the nearly pure partitioning of strain into components parallel and normal to the arc, as seen in other regions, is not occurring here: 1) the arc parallel strike-slip faults have a thrust component; 2) the imbricate thrust faults have a strike-slip component (as at Weber). Under this view, the normal faulting within the subducted plate is only a relict, the plate being pulled downward by its own weight.

Aftershock Behaviour and Precursory Features:

The numerous aftershocks of the February Weber mainshock decayed away in time more slowly than normal, although the b-value was not unusual. A close look at the rate of occurrence showed that there was a period of several weeks, immediately prior to the May mainshock, when the rate was very much lower than expected. Quiescence has been reported elsewhere before large earthquakes or, within aftershock sequences, before larger aftershocks. The Weber case cannot be explained away as being due to station faults, changes in analysis procedures, or prolonged periods of bad weather. Those aftershocks that did occur during this quiet period had magnitudes larger than normal (a low b-value). Low b-values have also been observed elsewhere before large events. The aftershocks of the May event behave in an entirely normal fashion.

The pairing of large events within a short time at Weber is not the only instance of this phenomenon. In 1942 two magnitude 7 events occurred in the Wairarapa with very similar epicentres but separated in depth. In that case the shallower event occurred some weeks before the deeper one, the reverse of the Weber case. Given this observed pairing, it would be well worthwhile keeping a closer than normal eye on the region of any similarly large event along the east coast. Real-time monitoring of the aftershock activity could detect any precursory changes as observed at Weber after the fact.

THE WEBER, NEW ZEALAND, EARTHQUAKE SEQUENCE OF 1990-1992

Russell Robinson
Seismological Observatory
N.Z. Institute of Geological & Nuclear Sciences, Ltd
P.O. Box 1320
Wellington, New Zealand

ABSTRACT

A series of four large earthquakes with epicentres very close to one another occurred in 1990-1992 in the Weber region of the southeast coast of the North Island, New Zealand. The region is one of oblique plate convergence and subduction, the plate interface being at about 20 km depth. The first event, February 19 1990, M_W 6.2, occurred within the upper part of the subducting Pacific plate on a steeply NW dipping normal fault, as defined by relocated aftershocks. The mechanism of this event reflects down-dip tension within the subducting plate due to "slab pull" forces, as is common in New Zealand. The second event, May 13 1990, M_W 6.4, occurred on an imbricate thrust fault in the overlying Australian plate, dipping shallowly NW, with a component of dextral strike-slip motion. The slip vector is close to the direction of plate convergence. Two subsequent large events, both of magnitude 5.5, occurred on August 15 1990 and March 2 1992, and extended the aftershock zone of the deeper first main shock to the NE, matching the extent of the shallower second main shock. Mechanisms of aftershocks of the two larger events are quite variable but as a whole are similar to the relevant mainshock. The time history of the aftershocks of the first (deeper) event shows a period of quiescence beginning 35 days before the second (shallow) event; the mean magnitude of those events that did occur was high. This cannot be explained by station faults, weather, or changes in analysis methods.

INTRODUCTION

Late in the afternoon of February 19, 1990, a strong earthquake (Weber I) was felt in the central east coast, North Island, New Zealand. Although the magnitude (M_L) was 6.1, damage was relatively minor, the intensity reaching MM 6 with one instance of MM 7 near the epicentre at the township of Weber (Figure 1a). There were many aftershocks felt. Approximately three months later, on the afternoon of May 13, a second strong shock was felt (Weber II, M_L=6.2), with a somewhat greater amount of damage. The maximum intensity was MM 8, with one exceptional instance of MM 9 (Figure 1b), again near Weber. As before, numerous aftershocks were felt. Routine determinations of the hypocentres of the two main shocks placed them very close to one another, but the depths of 31 km (February) and 17 km (May) were significantly different. No surface faulting was observed for either event (Berryman & Beanland, 1990). On August 18, 1990, a third event (Weber III) was widely felt in the region, but the magnitude (M_L=5.5) was too small to cause more than very minor damage. On March 2, 1992 a fourth large event (Weber IV) was felt, but again the magnitude (M_L=5.5) was not high enough to cause significant damage. Nevertheless, the residents of the region began to refer to themselves as living in the "earthquake capital of New Zealand". The routinely determined depths of both these later shocks were similar to that of Weber I.

Data gathered by the recently upgraded seismograph stations of the New Zealand Seismograph Network, and by temporary portable stations, make it possible to study this sequence of earthquakes in more detail than has previously been possible in New Zealand. The positions of the two largest events, the second almost directly above the first and three months later, provide an opportunity to search for possible precursory signals in the behaviour of the numerous aftershocks of the first event. The earthquakes are also important because of the tectonic setting: the subducting Pacific plate dips to the northwest at a shallow depth (about 20 km) under the region. The nature of the faulting involved should be indicative of how strain is taken up in this zone of oblique plate convergence. This paper will be concerned with the location of the main events and their aftershocks as redetermined using a suitable local velocity model. The distribution of events and focal mechanisms will be used to study the nature of the faulting involved and its tectonic implications. Temporal variations in two parameters of the Weber I aftershocks (mean magnitude, rate of activity) will be examined for unusual features related to the occurrence of Weber II. Some engineering aspects of the main shocks are discussed by Dowrick & Sritharan (in press). Anderson & Webb (in preparation) consider inversion of teleseismic waveform data for fault parameters. Webb (in preparation) considers some aspects of the foreshocks of Weber I. There is no geodetic information available on possible surface uplift or horizontal strain associated with the sequence; preliminary forward dislocation modeling suggests a maximum of 55 mm and 2.5 ppm (engineering strain) east of the epicentre for Weber II (Darby, as quoted in Barryman & Beanland 1990).

Geologic and Tectonic Setting

New Zealand lies in the convergence zone of the Australian and Pacific plates. In the North Island (Figure 2), this convergence in an east-west direction has resulted in subduction of the oceanic Pacific plate and a well developed Benioff-Wadati zone of mantle earthquakes reaching depths of about 300 km (Reyners, 1989). The southeast coast of the North Island, east of the main axial ranges, consists of a complex melange of Cenozoic marine sediments and isolated blocks of Mesozoic greywacke "basement". It is often referred to as an accretionary border. Topographically, it comprises a range of coastal hills ("outer-arc high") separated by a depression ("fore-arc basin") from the main greywacke ranges to the northwest. The oceanic lithosphere of the underlying Pacific plate appears to be thicker and more buoyant than normal (Robinson, 1986; Davy, in press), resulting in the exposure of a tectonic province usually found below sea level. The strike of the Hikurangi Trough, depth contours of deep seismicity, topographic trends, and major geologic structures are all roughly NE-SW, at an oblique angle relative to the E-W direction of plate convergence. Along the southeast coast, major strike-slip faults have developed that take up most of the arc-parallel strain, leaving the arc-normal strain to be accommodated by either thrusting on the plate interface, by imbricate thrust faults and folds above the interface both on and off shore, and a small thrusting component on the major strike-slip faults. Well defined terraces, inferred to be uplifted by events on the imbricate faults, are common along the east coast (Berryman et al, 1989). No large plate interface thrust events are known in the historic record: the two largest events (Figure 2) involved predominantly strike-slip motion in the overlying plate (1855, $M \approx 8$, on the Wairarapa fault; Grapes & Wellman, 1988) or a mixture of thrusting and strike-slip motion in the overlying plate (1931, $M \approx 7\ 3/4$; Haines, 1988).

In the Weber region (Figure 3) the major strike-slip Mohaka/Ruahine fault system bounds the axial greywacke ranges on the southeast. Dannevirke, the largest town in the region, lies to the east in the Manawatu river depression. In the coastal hills still further east active faults have been mapped (Berryman & Beanland, 1990), the largest being the NE striking dextral Waewaepa-Mangatoro-Oruawhara zone midway between Dannevirke and Weber. This system may be the northern continuation of the Wairarapa fault. There are minor normal faults still further east but little is known about them. In the coastal hills further to the northeast, in southern Hawke's Bay, detailed mapping (Cashman & Kelsey, 1990) has delineated NE-SW striking parallel zones of extension, contraction, and shear extending inland from the coast. On the coast southeast of Weber there is an exceptional lack of uplifted terraces (Berryman et al, 1989). The depth of the plate interface under the Weber region was estimated by Reyners (1980) at about 20 km. This was based on micro-earthquake locations determined from a temporary survey using portable instruments, the depth resolution of the permanent national network of seismographs being insufficient to do so. This depth is consistent with a similar survey by Kayal (1984) and a marine reflection profile off the east coast (Davey et al, 1986). Reyners (1983) later postulated segmentation of the subducting plate along strike, with one segment boundary lying northeast of the Weber region.

Regional Seismicity

The south/central east coast of the North Island is moderately active. Since 1964 (when epicentres began to be determined by computer), there have been 12 events, in addition to this latest sequence, of magnitude 5.0 or more, and 105 events of magnitude 4.0 or more, in a 100 x 100 km region centred on Weber. The largest was magnitude 5.8 in 1975, with a hypocentre about 25-30 km west of the Weber shocks at a depth of about 55 km (Figure 3). Routinely determined depths for these events extend from 9 to 103 km, but values of less than 50 km are not determined with sufficient accuracy to safely classify a particular event as to its tectonic situation: on, above, or below the plate interface. However, results from temporary micro- earthquake surveys suggest that the bulk of events occur within the upper reaches of the subducted Pacific plate lithosphere: this is clearly the case further south near Wellington where there is a denser network of permanent seismographs (Robinson, 1986). Such events have more-or-less evenly distributed epicentres and do not define specific fault zones. Their mechanisms reflect down-dip tension in the subducting plate (Arabasz & Lowry, 1980; Reyners, 1980; Kayal 1984; Robinson, 1986). Events above the plate interface have mechanisms reflecting east-west compression, in accord with geodetically determined strain accumulation (Walcott, 1978) and plate tectonic predictions.

Aside from the two major events in 1855 and 1931, discussed above, the largest historical event in the southeast coast region was the 1934 Pahiatua event with magnitude 7.6, probably about 60 km west-southwest of Weber. Little is known about this event: Eiby (pers. comm.) suggested that the depth was "not very shallow" since the maximum intensity, relative to the felt extent and instrumental magnitude, was too low. There were, however, a great many aftershocks so that a depth greater than about 50 km is unlikely. Even less (Eiby, 1968) is known about events in 1863 (felt over most of New Zealand; damage and ground fissures at Napier), 1917 in the northern Wairarapa, and 1930 (off the east coast but felt strongly). Two 1942 events with nearly identical epicentres in the Wairarapa, about 80 km to the southwest, both of magnitude about 7.0, are of particular interest here because of the pairing similar to the two largest Weber events. In the Wairarapa case, however, the first event was shallow and the second deeper (about 50 km; Eiby, 1968).

DATA SOURCES AND RELOCATION PROCEDURE

Data used in this study consist of readings made during routine analysis of records from the N.Z. National Seismograph Network and from temporary portable stations installed in the epicentral region. No teleseismic data were used except for focal mechanism solutions.

The New Zealand National Seismograph Network has recently undergone significant improvement. The once photographic or pen & ink recording instruments have been replaced with digitally recording systems with very high dynamic range (Gledhill et al, 1991), and the density of sites increased somewhat. The sampling frequency is 50 Hz; only short-period (1 Hz) seismometers are used. Recording is triggered, not continuous. Of the 22 permanent stations used for relocating events (Figure 2, Table 1) the closest was PGZ , 30 km south of Weber, with a single vertical component, bore-hole seismometer. Portable seismographs of two types were installed in the epicentral region for short periods (Figure 3, Table 1) after the two mainshocks in 1990 and after the fourth large event in 1992. The first type ("EARSS") is essentially a portable version of a 3-component permanent National Network instrument (but with 100 Hz sampling). The second type ("RATS", Robinson, 1988) does not record waveforms, only arrival-times, first-motions, and amplitudes.

The events selected for relocation include all those routinely placed within the rectangular region 40.00-40.75 S, 175.75-176.75 E, centred on Weber, from January 1, 1989 to March 31, 1992 (the latest available at the time of writing).

Seismic Velocity Model

Because of the complex structure of the Weber region and the variable number of stations available, it is important to have a reasonably good velocity model if event locations are to be comparable throughout the period considered and not biased according to the presence or not of any particular station. For this reason a velocity model has been derived using the technique of iterative inversion of arrival-time data for both hypocentres and velocity parameters (e.g. Crosson, 1976). The specific implementation used is described in detail by Robinson (1983, 1986). It is not possible to derive a fully 3 dimensional, or even 2 dimensional, model due to the the very restricted range of event positions during the periods of portable instrument deployment. The model used is 1-dimensional (i.e. flat layers) with a fixed P/S velocity ratio, plus station terms. Since the bulk of the events occurred in a small volume, such a model is probably not too unreasonable.

The data used to derive this model were the P and S arrival times of 243 well observed events that occurred during the periods of portable station deployment. The parameters of the shallowest two layers were fixed on the basis of preliminary results of a crustal refraction experiment along the east coast of the North Island (Reyners, pers. comm.); and a layer boundary was placed at the estimated depth of the plate interface (20, later 19 km). Left to itself, the velocity in the deep half-space does not converge, increasing to well over 9.0 km/sec. In the final model it has been set to 8.77 km/sec, the value found near Wellington (Robinson, 1986). The final model (Table 2) gives an r.m.s. travel-time residual (weighted by arrival quality) of 0.05 seconds; resolution of all free parameters is good (diagonal element of the resolution matrix of 0.90 or more, except for the WAH S term (0.75)). Not all of the more distant stations used in the later relocation of events were included in the inversion. For these distant sites station terms (Table 1) were derived by relocating a large number of additional events, using the above model and local stations only, and then setting the distant station terms equal to their average travel-time residuals after deletion of obviously bad readings. Additional small changes were made to station terms for a few of the original stations used in the inversion if results from this larger number of events warranted it.

Although the mapping of a real complex 3-D velocity structure into a 1-D model makes detailed interpretation unwise, the velocity model can be roughly interpreted as reflecting a near surface layer of Cenozoic sediments overlying a denser crust, perhaps greywacke grading down to schist. The interface between the Australian and Pacific plates, at about 19 km depth, is marked by a velocity reversal, perhaps in part due to some thickness of subducted marine sediments overlying the oceanic crust (Davey et al, 1986). The station terms for the local sites generally increase towards the coast and to the NE, reflecting a thickening of low velocity sediments in those directions.

Magnitude Determination

Magnitudes are determined using the amplitude-magnitude relationship derived for the Wellington region (Robinson, 1986); Wellington is similar tectonically to the Weber region and the range of distances is much the same. For some of the purposes of this study it is necessary to have a complete catalogue of events above some minimum magnitude. Thus, as for locations, station terms are required so that individual event magnitudes are not unduly biased by the specific set of stations used. These terms (Table 1) were determined by adopting as a reference magnitude the average at 7 stations of the Wellington Network, stations at which there were no known instrumental changes or faults likely to affect their gain. Average magnitude residuals, relative to this reference, for the entire set of relocated events were used as station terms.

Location Quality

A total of 4151 events were relocated using the velocity model and magnitude terms discussed above, after discarding a few small events with insufficient data. Obviously bad readings in the located events were corrected or deleted. The events were assigned quality ratings, A-D or F, according to various criteria (Table 3). The percentage of events in each class were: A 12%, B 19%, C 22%, D 43%, F 4%. Almost all quality A events occurred during the periods of portable instrument deployment. Quality F events were mostly small events which failed to converge to a reasonable solution and whose hypocentres were set to that of the most recent mainshock; they are not shown in the following figures or used for statistical purposes.

HYPOCENTRE DISTRIBUTION

Spatial Distribution

Map and cross-section views (Figure 4) of the entire data set, January 1989 - March 1992, quality A-D, show two regions of intense aftershock activity superimposed on the normal ongoing seismicity, most of which occurs within the upper part of the subducting Pacific plate at depths between 15 and 30 km with a lesser concentration still deeper, near 50 km. (This "double band" nature of the seismicity in the Pacific plate is clearer near Wellington, where a broader region can be considered; Robinson, 1986.) The activity near 50 km depth appears to be more intense near the down dip extension of the Weber I fault zone.

The sharpening of detail expected with increase in event quality makes it possible to use quality A events to estimate the strike and dip of the faults involved in the Weber I and II shocks. This is done by examining a series of cross-sections made at a range of rotations. Events used are those within a 40 x 40 x 40 km volume centred at 41.315 S, 176.325 E, with N45E taken as the 0 rotation reference. A choice made "by eye" on the basis of apparent fit to a single plane, gives a strike and dip of N50E, 75° NW for Weber I and N35E, 35° NW for Weber II with an uncertainty of about 5. Attempts to determine the best strikes and dips using a least- squares fit of a plane to the hypocentres require a subjective restriction of the events used to those thought to lie on "the plane". Also, for Weber II there may be some curvature. Nevertheless, if this is done the results are within a few degrees of the above estimates (N48E and N38E for Weber I and II respectively). Composite cross-sections constructed using a rotation (from N45E) of 10° for events less than 19 km deep and -5° for events greater than 19 km deep (Figure 5) give a good picture of the fault geometry.

There were no portable instruments deployed after the Weber III event, so that a strictly equivalent procedure can not be used to determine the strike and dip of the fault involved. Four portable instruments (1 EARSS and 3 RATS) were deployed after Weber IV, but still the limited number means that few (13) events were classified as A quality. To further examine the position of these two events relative to Weber I and II, class A and B events (Figure 6) are used. The aftershock zone of Weber III overlaps the northeastern end of the aftershock zone of Weber I and extends it somewhat to the northeast. The aftershock zone of Weber IV both overlaps the northeastern end of the Weber III zone and extends it still further northeast and up. The extent, NE-SW, of the combined Weber I,III, and IV aftershock zones seems to match the extent of the overlying Weber II zone. The Weber mainshocks themselves (Table 4, Figure 5 and 6) were not particularly well located, event qualities of C,D,C,B being assigned given the criteria in Table 3. The D rating for Weber II is due to the lack of any credible S readings. The Weber II hypocentre is located somewhat off the apparent fault plane, in a NW direction, as defined by the best located aftershocks. This is typical of many quality D hypocentres (Figure 4), and is unlikely to be real.

Time and Magnitude Distribution

For the purposes of examining the time history of events and various statistical parameters, only events clearly associated with the Weber events were used, i.e. events with (relocated) hypocentres falling within a 40 x 40 x 40 km volume centred on the Weber I and II aftershock zones (Figure 3). Events with depths of less than 19 km were associated with Weber II; deeper events with Weber I, III, and IV. An overview of the activity (Figure 7), separated into depth ranges appropriate for Weber I and II, shows no apparent change in rate of activity in the year prior to Weber I. There was 1 immediate foreshock $10^1/_2$ hours prior to the main event. Apparently there was some induced activity after Weber I in the region close to the eventual Weber II event, although some of this may be due to location error. The Weber II event had 6 foreshocks in the preceding day. The mainshock seems to have induced a fair number of events in the Weber I aftershock zone. The Weber III and IV events both induced their own aftershock sequences.

In order to examine various statistics of the event sequence it is necessary to have a catalogue that is substantially complete down to some minimum magnitude. In order to determine the magnitude cutoff it is customary to use a plot of cumulative event frequency as a function of magnitude. The magnitude threshold is taken as the point at which the curve deviates from linearity. The periods with portable instrument coverage must be excluded since the detection threshold would have been much lower than normal. Deep and shallow activity have also been considered separately (Figure 8). From the figure, a magnitude threshold of 2.65 for both deep and shallow activity seems appropriate and has been adopted for all subsequent work.

The "b-value" is the negative of the slope of the linear section of the frequency-magnitude plot, but is usually calculated using the maximum likelihood formula:

$$b = \frac{\log(e)}{(M_{av} - M_{min})} \qquad (1)$$

with errors of

$$\pm \frac{b}{n^{1/2}} \qquad (2)$$

where M_{min} is the cutoff magnitude, M_{av} is the average magnitude, and n is the number of events. Data for the Weber region, 890101-920331 (including the periods with portable instruments), M≥2.65, give a b-value of 1.01±0.04 (544 events) for events with depth ≥19.0 km. The same formula can be applied to the shallower activity (b=0.77±0.03, 504 events) but figure 11 shows that the frequency-magnitude plot is not linear, there being a change in slope at about magnitude 3.75, well above the detection threshold. This persists when data during the periods with portable instruments is included. The b-values for the two segments are 0.62±0.01 and 1.35±0.06 (from a least squares regression). The reason for this break in slope is not known. Jin & Aki (1989) explain a similar breakdown in self-similarity on the basis of a characteristic length scale in a creep model of fracture.

The overall time history of an aftershock sequence is usually specified by the "p-value" in the Omori law of rate decay:

$$n(t) = n(1) \times t^{-p} \tag{3}$$

where n(1) is the rate of activity after 1 day, and t is the time in days. The results for Weber I and II (Figure 9) are within the normal range but significantly different: p=1.126±0.021 for events with depth <19 km from the time of Weber II up to 920401; and p=0.847±0.028 for events with depth ≥19 km from the time of Weber I up until the time of Weber III. In the case of the deeper activity, the Weber II, III, and IV events all induced a temporary increase in rate above that expected from a simple extrapolation.

FOCAL MECHANISMS

Weber I

Centroid-moment tensor solutions (Table 5), based on teleseismic wave-form data, for Weber I, II, and III have been determined as part of the routine world-wide program at Harvard University (Dziewonski et al, 1991a; 1991b; 1991c). Teleseismic and local first motion data for Weber I are generally consistent with the best fitting double-couple mechanism (figure 10a), despite the notorious unreliability of teleseismic short-period readings. The mechanism includes a NE striking, steeply dipping nodal plane which is close to that found from the distribution of aftershocks. However, the first motion data can be better matched by a nodal plane still closer to that implied by the aftershocks and a more substantial rotation of the other plane. Some distortion of the true take-off angles and azimuths could be expected because of the 3-D nature of the local structure. Still, it is clear that a mechanism involving primarily dip-slip motion on a fault striking NE and dipping steeply to the NW is required.

Many of the Weber I aftershocks were well recorded during the short period of portable instrument deployment. Despite the small number of instruments, the coverage of the focal sphere is adequate, for a well observed event, to usefully constrain a focal mechanism solution. However, because of the small number of stations there is a possibility of a single incorrect observation affecting the nature of the allowable mechanisms considerably. An additional problem is that there is often some doubt as to the direct/refracted nature of arrivals at MNG: observations that are inconsistent with data from closer stations when interpreted strictly according to the computed take-off angle would not be so if interpreted as a direct rather than refracted arrival. For this reason data from MNG have not been used for aftershock mechanisms.

Aftershocks with a sufficient number and distribution of polarity observations to reasonably constrain a mechanism were considered for individual solutions; 43 mechanisms were obtained (Table 6). Although mainly of normal-fault type, the dip and strike of the nodal planes varied widely. Figure 11a attempts to summarize the results by plotting the distribution of the P and T axes. Both occur in clusters: the P axes tend to be close to vertical or, if not, strike roughly east-west; the T axes are generally closer to horizontal in an NW-SE direction. The P and T axes obtained from a mechanism represent the axes of principal strain, not stress. However, for a large number of events with varying fault plane orientations, the predominant orientation of the P and T axes can be taken as representative of the principal stress directions also. As is the case with the normal seismicity elsewhere along the SE coast, these results probably reflect down-dip tension in the subducting Pacific plate.

Weber II

The best double-couple fit to the Harvard moment tensor solution for Weber II agrees reasonably well with the first motion data (Figure 10b; the reading at TEH is the obvious misfit at a NW azimuth). A nodal plane with a strike set to that of the aftershocks (N35E) seems to fit better although a dip somewhat greater (40 vs 35° NW) is required to get the best agreement. Both mechanisms imply primarily reverse faulting with a varying degree of dextral strike-slip motion.

Because of the greater number of portable instruments deployed after Weber II, a greater number of aftershocks (105) provided reasonably constrained mechanisms (Table 6). Again there was a wide range in strike and dip of the nodal planes. A summary of the distribution of P and T axes (figure 11b) indicates that the P axes tend to be semi-horizontal and strike in a NW-SE or E-W direction. The T axes are more widely spread but generally strike in a N-S direction if not nearly vertical. The "typical" P axis is somewhat rotated (clockwise) from the direction of plate convergence, as expected for strain in an oblique convergence situation (Darby, pers. comm.).

Weber III and IV

These events have magnitudes near the lower limit of those that can be expected to provide good teleseismic data for moment tensor inversion or for first motion observations. The published best double-couple moment tensor solution (Dziewonski et al, 1991c) for Weber III (Table 5) involves nearly pure normal faulting on NE striking nodal planes, one of which is close to the position of the plane defined by the combined Weber I, III, and IV aftershocks. At the time of writing there has been no moment tensor solution published for Weber IV. The local first motion data are very similar to those for Weber I. Until more data become available it is assumed that the mechanism is similar to that for Weber I, i.e. normal faulting on a NE striking, steeply dipping plane. There is insufficient coverage from portable instruments to allow mechanisms to be obtained for aftershocks of either Weber III or IV.

TEMPORAL VARIATIONS IN AFTERSHOCK PROPERTIES

Because of the relative positions of the Weber I and II hypocentres, the latter almost directly above the former, there is an opportunity to look for precursory features of the deeper Weber I aftershocks. The location errors during periods of no portable instrument coverage are too large to permit detailed investigation of hypocentre clustering or migration. However, changes in rate of activity and b-value (or equivalently in mean magnitude) can be examined. A study of coda Q variations is still in progress and will be presented separately.

Rate of Activity

Various investigators have suggested that changes in rate of activity (generally quiescence) are related to either forthcoming main shocks (see Habermann, 1988 for a review) or, within an aftershock sequence, to larger aftershocks (e.g. Matsu'ura, 1986). Logarithmic plots of rate of activity vs time, such as in Figure 9, are uninformative because of the very large range of time intervals used. As in Matsu'ura (1986) it is better to consider deviations in more detail by comparing, event by event, the (observed) accumulated number of aftershocks with the number expected given the overall rate of decay as expressed in the Omori relationship (3) discussed above. The results for the Weber I aftershocks (Figure 12) show that the deviation from the expected number stabilizes very soon after the main shock and stays so for about 45 days. There is then a 12 day period with no activity, followed by a period of less than expected activity up until the occurrence of Weber II. The rate then increases, bringing the accumulated number back up to the expected level where it then remains.

Mean-Magnitude

Various investigators have suggested that changes in b-value with time are related to either forthcoming main shocks (e.g. Smith, 1986; Imoto, 1991) or, within an aftershock sequence, to larger aftershocks (Gibowicz, 1973). It is more convenient here to consider changes in mean magnitude, which is inversely related to the b-value (equation 1). In an uncomplicated situation the mean magnitude is expected to decay gradually with time, reflecting stress relaxation, as observed for instance following the 1986 Edgecumbe earthquake (Smith & Oppenheimer, 1986).

A plot of mean magnitude vs time (Figure 13) for the Weber I aftershock activity shows that during the first five or so days there is a wide range of values, the initial unrealistically high values probably reflecting the missing small magnitude events in the first few hours after the main shock. The mean then appears to decrease gradually over the next 20 days in the expected fashion. It then appears to increase prior to Weber II, then falls afterwards. It is also interesting to note the high value of mean magnitude for the year preceding the main Weber I shock.

DISCUSSION

The results presented above for the fault geometry and mechanism of the Weber earthquakes can be combined with the velocity model to derive a structural and tectonic model of the region involved (Figure 14). It confirms previous ideas: that at least part of the arc normal strain due to oblique plate convergence is taken up by faulting on imbricate thrusts above the plate interface. Such faulting, at least in this case, also includes a component of strike-slip motion, resulting in a slip-vector with direction close to that of plate convergence. In the case of Weber II the faulting did not reach the surface, being confined to the more competent crust at depth. This so called "blind thrusting" (Stein & Ekstrom, 1992) would be expected to manifest itself on the surface by folding. While the velocity structure certainly is more complex in detail than depicted in Figure 14 (e.g. isolated blocks of upfaulted greywacke "basement" do appear on the surface east of the main ranges) the general picture is one of increasing thicknesses of low velocity sediment coastwards. The underlying more competent crust can be considered as forming the "backstop" in plate tectonic terminology.

The deeper Weber I (and III and IV) events are larger examples of the pervasive normal faulting found to be typical within the upper reaches of the subducting Pacific plate in New Zealand. This type of faulting is usually explained as a consequence of the "slab pull" force arising from the deeper subducted lithosphere. This force is resisted by friction along the plate interface, and perhaps, at shallow depth, by the thicker than normal nature of the subducting oceanic crust. The question of the occurrence or not of large plate interface thrusting events remains unanswered. The most likely such event in historical times would be the 1934 Pahiatua earthquake (magnitude $7^1/_2$) but little is known with certainty about even its location, much less its mechanism. It is not known for how long thicker than normal oceanic crust has been subducting and it is conceivable that large interface events are now rare, leaving the convergence to be taken up largely by other means.

The close temporal relation of the Weber I and II shocks is unlikely to be pure coincidence. The intimate relation of the Weber events to one another is supported by the close correspondence in extent of the aftershock zones (Weber II vs Weber I + III + IV). The two magnitude 7 Wairarapa events in June and August of 1942 are another example, but with the shallower event occurring first (there was a closely associated third event, magnitude 6.0, in December, at shallow depth). It should be noted, however, that such pairing is by no means the rule: the magnitude 6.0 Cape Campbell earthquake near Wellington in 1977 occurred within the subducting Pacific plate at a depth of about 40 km but was not followed by a similarly large shallow event. The precise mechanism of how one event sometimes triggers the next is unclear. The time delay between paired events (83 days in 1990, 37 days in 1942) suggests that more than simple elastic effects are involved. Clustering of large events in general is becoming recognized as more common than previously thought (e.g. Kagan & Jackson, 1991). An example of particular relevance is the sequence of 3 "hidden" thrust events, 1982-1985, in the coast ranges of central California (Stein and Ekstrom, 1992). These events (magnitudes 5.4, 6.5, and 6.1) abutted and migrated southward over a distance of 65 km.

The Weber I event had numerous aftershocks whose rate of occurrence decayed slowly with time. Not all events within the subducting Pacific plate at relatively shallow depths (say less than 50 km) do so. The Cape Campbell event mentioned above had few aftershocks. That event was located in the lower band of the double-banded seismicity typical of the subducted plate; events with numerous aftershocks seem to occur in the upper band (as at Weber; for other examples see Bannister et al (1989), Reyners (1983). The 1982 Hawke's Bay event (M_L 5.6) seems to be an exception (Reyners, 1984).

There are indications that the normal progression of aftershocks following the Weber I event was interrupted about 35 to 40 days before the occurrence of Weber II: quiescence and an increase in mean magnitude of the events that did occur. Quiescence in the background seismicity has been documented before several large earthquakes (Habermann, 1988) and within aftershock sequences (Matsu'ura, 1986). Gibowicz (1973) reported decreases in b-value (equivalent to an increase in mean magnitude) within several New Zealand aftershock sequences before the occurrence of large aftershocks. Apparent quiescence and an increase in mean magnitude could both be explained by an upward change in detection threshold. Such a change could be caused by a critical station being inoperative or to prolonged periods of windy conditions. However, during the period in question, all of the "local" stations were operating normally. Data on wind conditions at all the various sites are not readily available, but monthly wind-run values at Wellington (which should be indicative of conditions on the southeast coast generally) for March through May 1990 are below normal (New

Zealand Meteorological Service, 1990abc). Also, replotting Figure 12 for different values of the magnitude threshold, from 2.55 to 2.95, shows that the quiescent period is still present.

Given the observed pairing of large events along the southeast coast of the North Island, keeping a closer than normal watch on the region of any future large event would be justified. If real-time monitoring of aftershock parameters were available, then some warning of a possible second large event might be possible.

ACKNOWLEDGEMENTS

I am grateful to Diane Maunder for her assessment of felt intensity reports and the drawing of the isoseismal maps. The deployment of portable instruments was carried out by many members of the Geology and Geophysics Division, DSIR, and the Institute of Geophysics, Victoria University: thanks to all involved. Also, this study would not have been possible without the conscientious performance of the routine analysis team. T. Webb provided many invaluable bits of information re station performance, data extraction programs, and focal mechanism plotting programs. The New Zealand Earthquake and War Damage Commission provided a grant without which this research would not have been done.

REFERENCES

Anderson, H.A. & Webb, T. (in preparation). (..Title to be filled in when available...).

Arabasz, W.J. & Lowry, M.A., 1980. Microseismicity in the Tararua-Wairarapa area: depth varying stresses and shallow seismicity in the southern North Island, New Zealand. *New Zealand Journal of Geology and Geophysics, 23*: 141-154.

Bannister, S.C., Perin, B.J. & Webb, T.H., 1989. Normal faulting through subducted oceanic crust: the 19 July 1985 earthquake of Hawke's Bay, New Zealand. *Tectonophysics, 162*: 303-313.

Berryman, K.R., Ota, Y. & Hull, A.G., 1989. Holocene paleoseismicity in the fold and thrust belt of the Hikurangi subduction zone, eastern North Island, New Zealand. *Tectonophysics, 163*: 185-195.

Berryman, K. & Beanland, S., 1990. Reconnaissance of the epicentral area of May 13, 1990 "Weber 2" earthquake, Dannevirke district. *EDS Immediate Report 90/5*, New Zealand Geological Survey, Wellington.

Cashman, S.M. & Kelsey, H.M., 1990. Forearc uplift and extension, southern Hawke's Bay, New Zealand: Mid-Pleistocene to present. *Tectonics, 9*: 23-44.

Crosson, R.S., 1976. Crustal structure modelling of earthquake data, 1: Simultaneous least squares estimation of hypocentres and velocity parameters. *Journal of Geophysical Research, 81*: 3036-3046.

Davey, F.J., Hampton, H., Childs, J., Fisher, M.A., Lewis, K., & Pettinga, J.R., 1986. Structure of a growing accretionary prism, Hikurangi margin, New Zealand. *Geology, 14*: 663-666.

Davy, B.W. (In press). The influence of the subducted plate buoyancy on the subduction of the Hikurangi-Chatham Plateau beneath the North Island, New Zealand. *In*: Advances in the Geology and Geophysics of the Continental Margin, American Association of Petroleum Geologists Memoir 53.

Dowrick, D.J. & Sritharan, S. (In preparation). Attenuation of peak ground accelerations in some recent New Zealand earthquakes.

Dziewonski, A.M., Ekstrom, G., Woodhouse, J.H. & Zwart, G., 1991a. Centroid-moment tensor solutions for January-March, 1990. Physics of the Earth and *Planetary Interiors, 65*: 197-206.

Dziewonski, A.M., Ekstrom, G., Woodhouse, J.H. & Zwart, G., 1991b. Centroid-moment tensor solutions for April-June, 1990. *Physics of the Earth and Planetary Interiors, 66*: 133-143.

Dziewonski, A.M., Ekstrom, G., Woodhouse, J.H. & Zwart, G., 1991c. Centroid-moment tensor solutions for July-September, 1990. *Physics of the Earth and Planetary Interiors, 67*: 211-220.

Eiby, G.A., 1968. An annotated list of New Zealand earthquakes, 1460 - 1965. *New Zealand Journal of Geology and Geophysics, 11*: 630-647.

Gibowicz, S.J., 1973. Variation of the frequency-magnitude relation during earthquake sequences in New Zealand. *Bulletin of the Seismological Society of America, 63*: 517-528.

Gledhill, K.R., Randall, M.J. & Chadwick, M.P., 1991. The EARSS digital seismograph: system description and field trials. *Bulletin of the Seismological Society of America, 81*: 1380-1390.

Grapes, R. & Wellman, H. 1988. The Wairarapa Fault. *Research School of Earth Sciences Publication Number 4*, Victoria University of Wellington, Wellington.

Habermann, R.E., 1988. Precursory seismic quiescence: past, present, and future. *Pure and Applied Geophysics, 126*: 279-318.

Haines, A.J., 1988. Deducing source properties of the M=7.8 1931 Hawke Bay, New Zealand, earthquake from the pattern of uplift and subsidence (abstract). *Earthquake Research Letters, 59*: 36.

Imoto, M., 1991. Changes in the magnitude-frequency b-value prior to large (M≥6.0) earthquakes in Japan. *Tectonophysics, 193*: 311-325.

Jin, A. & Aki, K., 1989. Spatial and temporal correlation between coda Q and seismicity and its physical mechanism. *Journal of Geophysical Research, 94*: 14041-14059.

Kagan, Y.Y. & Jackson, D.P., 1991. The seismic gap hypothesis: ten years after. *Journal of Geophysical Research, 96*: 21419-21431.

Kayal, J.R., 1984. Microseismicity and tectonics at the Indian/Pacific plate boundary: south-east Wellington province, New Zealand. *Geophysical Journal of the Royal Astronomical Society, 77*: 567-592.

Matsu'ura, R.S., 1986. Precursory quiescence and recovery of aftershock activity before some large aftershocks. *Bulletin of the Earthquake Research Institute of Tokyo University, 16*: 1-65.

New Zealand Meteorological Service, 1990a. Wellington Weather Summary, March 1990.

New Zealand Meteorological Service, 1990b. Wellington Weather Summary, April 1990.

New Zealand Meteorological Service, 1990c. Wellington Weather Summary, May 1990.

Pho, H.T. & Behe, L., 1972. Extended distances and angles of incidence of P waves. *Bulletin of the Seismological Society of America, 62*: 885-902.

Reyners, M., 1980. A microearthquake study of the plate boundary, North Island, New Zealand. *Geophysical Journal of the Royal Astronomical Society, 63*: 1-22.

Reyners, M., 1983. Lateral segmentation of the subducted plate at the Hikurangi margin, New Zealand: Seismological evidence. *Tectonophysics, 96*: 203-223.

Reyners, M., 1984. The Hawke's Bay, New Zealand, earthquake of 1982 September 02 and deformation in the interior of the subducted Pacific plate. *Tectonophysics, 106*: 259-273.

Reyners, M., 1989. New Zealand seismicity 1964-1987: an interpretation. *New Zealand Journal of Geology and Geophysics, 32*: 307-315.

Robinson, R., 1983. Velocity structure of the Wellington region, New Zealand, from local earthquake data and its implications for subduction tectonics. *Geophysical Journal of the Royal Astronomical Society, 75*: 335-359.

Robinson, R., 1986. Seismicity, structure, and tectonics of the Wellington region, New Zealand. *Geophysical Journal of the Royal Astronomical Society, 87*: 379-409.

Robinson, R., 1988. "RATS": an inexpensive portable earthquake recorder (abstract). Seismological Research Letters, 59: 21.

Smith, E.G.C. & Oppenheimer, C.M.M., 1989. The Edgecumbe earthquake sequence: 1987 February 21 to March 18. *New Zealand Journal of Geology and Geophysics, 32*: 31-42.

Smith, W.D., 1986. Evidence for precursory changes in the frequency-magnitude b-value. *Geophysical Journal of the Royal Astronomical Society, 86*: 815-838.

Stein, R.S. & Ekstrom, G., 1992. Seismicity and geometry of a 110 km-long blind thrust fault, 2, Synthesis of the 1982 - 1985 California earthquake sequence. *Journal of Geophysical Research, 97*: 4865-4883.

U.S. Department of the Interior, Geological Survey, 1990a. *Earthquake Data Report 2-90*, part 2.

U.S. Department of the Interior, Geological Survey, 1990b. *Earthquake Data Report 5-90*, part 1.

U.S. Department of the Interior, Geological Survey, 1990c. *Earthquake Data Report 8-90*, part 1.

Walcott, R.I., 1978. Geodetic strains and large earthquakes in the axial tectonic belt of North Island, New Zealand. *Journal of Geophysical Research, 83*: 4419-4429.

Webb, T.H. (in preparation) Spatial clustering and stress drops of foreshocks of the 1990 February Tennyson and Weber, New Zealand, earthquakes.

TABLE 1: Station List

CODE	DATES	LAT °S	LON °E	TYPE	P-TERM sec.	S-TERM sec.	M-TERM
AGA	900220-900222	40.4533	176.4797	LE3	0.24	0.60	0.93
AGA2	900514-900517	40.4533	176.4797	LE3	0.24	0.60	2.05
AGA3	920302-920330	40.4533	176.4797	LE3	0.24	0.60	-
BHW	P	41.4092	174.8714	DW1	-0.35	-	-
BLW	P	41.3686	175.4747	DW1	-0.30	-	-1.04 R
BRR	900514-900517	40.2053	176.6058	LR1	0.33	0.21	-
C03	920302-920330	40.2869	176.1794	LR1	-0.08	-0.04	-
CAW	P	41.1089	175.0678	LW1	0.00	-	-1.06 R
CCW	P	41.7508	174.2169	DW1	0.43	-	-
CLH	900515-900517	40.2039	176.2583	LR1	0.03	0.29	-
HAT	P	38.8922	176.0919	DT1	1.74	-	-
HNH	P	39.6653	176.8811	DH1	-	2.00	1.27
HOP	900514-900518	40.3508	175.9575	LR1	-0.16	-0.23	-
KHZ	P	42.4181	173.5403	DE3	-0.12	-	1.68
KIW	P	40.8639	174.9117	LW1	0.68	-	-0.71 R
MAR	900221-900222	40.4236	176.0339	LE3	-0.27	-0.44	0.97
MKO	900515-900517	40.4292	176.0925	LE3	-0.04	0.19	1.48
MNG	P	40.6186	175.4819	LE3	0.07	-0.11	1.01
MOW	P	41.4217	175.2519	DW1	-0.53	-	-0.80 R
MRW	P	41.2325	174.7050	DW3	0.11	0.55	-1.01 R
MTW	P	41.1594	175.5019	LW3	-0.47	-	-
ORE	900515-900517	40.0614	176.3731	LE3	-0.01	0.15	2.36
PGZ	P	40.6189	176.2736	LE3	-0.01	-0.04	1.42
PNH	900515-900517	40.3394	176.6400	LE3	0.56	0.62	1.96
POR	900219-900222	40.3144	176.6069	LR1	0.44	-	-
PUZ	P	38.0733	178.2572	DE3	-	3.50	1.94
RAT	P	38.8686	175.7711	DT1	-	-	-0.67
RDM	900514-900518	40.1069	176.0694	LE3	-0.11	-0.04	1.69
RTR	900514-900517	40.1603	176.4261	LR1	0.15	0.20	-
SKR	900514-900517	40.3775	176.4689	LR1	-0.01	0.58	-
TAH	P	39.1358	176.7403	DH1	1.37	-	-
TAX	900219-900220	40.4131	176.3322	LR1	0.02	0.08	-
TCW	P	41.2133	174.2758	DW1	0.35	-	-0.79 R
TEH	P	39.9894	176.8111	LH1	0.57	-	-0.49
TEU	900220-900222	40.2503	176.3578	LE3	0.00 R	0.26	1.03
TEU2	900513-900517	40.2503	176.3578	LE3	0.00	0.26	1.31
TEU3	920302-920330	40.2503	176.3578	LR1	0.00	0.26	-
TTH	P	39.5414	176.8261	DH1	0.91	-	-0.24
TTW	920302-920330	40.3228	176.4278	LR1	-0.01	0.58	-
WAH	P	39.6992	176.3553	LH1	0.50	1.20	-0.86
WBR	900513-900517	40.4081	176.2878	LE3	-0.03	0.03	1.18
WDW	P	41.2686	174.9936	DW1	-0.35	-	-1.25 R
WEB	900221-900222	40.4061	176.2922	LR1	0.07	0.33	-
WEL	P	41.2861	174.7683	DE3	0.04	-	-
WTA	900219-900223	40.2922	176.1797	LE3	-0.08	-0.04	1.67
WTA2	900513-900517	40.2922	176.1797	LE3	-0.08	-0.04	1.63

P-TERM = station term for P arrivals; S-TERM = station term for S arrivals; M-TERM = station term for magnitudes. A "P" in the dates column=permanent. TYPE codes: L = local; D = distant; E = EARSS; R=RATS; W,N, or T: telemetered network, Wellington, Hawke Bay, or Taupo; 1 or 3 = number of components (1 = Z only). A "-" in any term column indicates that the station was not used for that purpose. An "R" indicates a reference site.

TABLE 2: Velocity Model

Depth, km	Vp, km/sec
0.0 - 4.0	3.55 *
4.0 - 8.0	5.35 *
8.0 - 13.0	5.94 ± 0.06
13.0 - 19.0	6.29 ± 0.06
19.0 - 25.0	6.10 ± 0.09
25.0 - 35.0	7.49 ± 0.08
35.0 -	8.77 *

* = fixed (see text)

TABLE 3: Location Quality Criteria

Quality =	A	B	C	D	F
Distance to Nearest Station, km	≤ Depth	≤ 2*Depth	≤ 3*Depth	> 3*Depth	> 3*Depth
Number of Stations	≥ 6	≥ 5	≥ 4	3	3
RMS Travel-Time Residual, Sec.	≤ 0.10	≤ 0.15	≤ 0.25	≤ 0.50	> 0.50
Number of Phases	≥ 8	≥ 6	≥ 5	≥ 4	4
Convergence	Yes	Yes	Yes	Yes	No
S.E. of X and Y, km	≤ 0.5	≤ 1.0	≤ 1.5	> 1.5	> 1.5
S.E. of Depth, km	≤ 1.0	≤ 2.0	≤ 3.0	> 3.0	> 3.0
S.E. of Origin Time	≤ 0.05	≤ 0.10	≤ 0.15	> 0.15	> 0.15
At Least One S Phase	Yes	Yes	Yes	No	No

TABLE 4: Main Shock Parameters

Event	Date	Time	Lat. °S	Lon. °E	Depth km	Q	M_L	M_b	M_s	M_w
Weber I	900219	053437.65	40.362	176.355	24.23	C	6.05	5.9	6.3	6.2
Weber II	900513	042309.25	40.281	176.301	11.92	D	6.24	6.0	6.3	6.4
Weber III	900815	155443.36	40.322	176.435	30.85	C	5.52	5.4	5.0	5.2
Weber IV	920302	090556.76	40.311	176.475	24.23	B	5.54	-	-	-

TABLE 5: Main Shock Mechanisms

Event	Best Double Couple			First Motion Fit			Aftershock Prediction	
	Strike	Dip	Rake	Strike	Dip	Rake	Strike	Dip
Weber I	209	72	-112	225	75	-70	230	75
	82	28	319	350	25	218		
Weber II	220	28	149	215	40	160	215	35
	-22	76	66	-39	77	52		
Weber III	233	56	260	-	-	-	-	-
	72	35	75					

TABLE 6: Aftershock Principal Axes

Weber I:

Num.	Azimuth			Angle		
	P	T	B	P	T	B
173	-42.30	141.37	50.15	35.19	54.87	88.27
214	-59.75	138.72	46.35	21.64	69.38	83.72
227	-30.00	150.00	60.00	30.00	60.00	90.00
251	-51.00	137.75	45.49	30.71	59.59	86.16
254	-51.00	137.75	45.49	30.71	59.59	86.16
283	134.77	46.52	-18.02	75.88	96.93	15.79
284	99.64	-156.33	-175.26	81.58	31.40	120.00
300	-22.06	160.92	70.17	30.08	59.95	88.71
324	0.00	-180.00	90.00	0.00	90.00	90.00
361	-44.08	141.83	50.33	30.32	59.82	87.42
425	-51.00	137.75	45.49	30.71	59.59	86.16
449	-37.06	145.92	55.17	30.08	59.95	88.71
458	49.01	-39.01	95.00	100.55	79.45	15.00
502	-37.06	145.92	55.17	30.08	59.95	88.71
513	-61.00	127.75	35.49	30.71	59.59	86.16
548	-20.00	160.00	70.00	30.00	60.00	90.00
549	-160.00	-160.00	110.00	20.00	110.00	90.00
607	109.14	154.05	-157.63	103.77	19.08	102.95
618	-165.00	-165.00	105.00	15.00	105.00	90.00
624	-59.94	159.26	67.62	13.83	79.19	81.46
634	0.00	-180.00	90.00	30.00	60.00	90.00
650	19.88	-12.02	-93.97	32.57	118.47	75.52
675	113.54	159.74	-137.33	125.23	45.57	114.90
688	84.64	168.04	71.73	44.70	96.49	133.97
693	97.17	-53.32	-171.78	79.64	11.86	84.28
697	-15.00	165.00	75.00	35.00	55.00	90.00
730	-51.00	137.75	45.49	30.71	59.59	86.16
752	-15.00	165.00	75.00	10.00	80.00	90.00
811	-51.00	137.75	45.49	30.71	59.59	86.16
829	-40.00	140.00	50.00	25.00	65.00	90.00
841	87.23	170.80	71.03	51.47	98.01	140.33
853	-79.01	99.23	9.96	40.08	49.93	90.87
864	-61.00	127.75	35.49	30.71	59.59	86.16
904	-50.00	130.00	40.00	40.00	50.00	90.00
929	-15.00	-15.00	75.00	135.00	45.00	90.00
998	142.34	172.58	-117.66	123.36	37.30	104.77
999	-84.03	-176.80	85.74	58.80	85.43	31.61
1031	-59.75	138.72	46.35	21.64	69.38	83.72

Weber II:

Num.	Azimuth			Angle		
	P	T	B	P	T.	B
1808	117.95	-148.54	-152.11	89.56	7.06	97.05
1811	115.00	115.00	-155.00	115.00	25.00	90.00
1829	100.00	100.00	-170.00	120.00	30.00	90.00
1836	117.95	-148.54	-152.11	89.56	7.06	97.05
1842	107.85	149.33	-160.78	99.49	12.57	98.18
1848	125.46	27.40	-95.08	65.99	72.53	30.38
1851	-70.00	-70.00	20.00	135.00	45.00	90.00
1852	78.95	149.11	173.90	100.18	27.89	115.66
1857	116.11	128.28	-151.71	114.84	25.34	94.70
1858	64.36	9.20	150.31	102.82	21.72	72.77
1866	-56.40	48.29	-15.34	56.73	68.87	138.97
1873	110.00	0.00	-160.00	90.00	0.00	90.00
1883	-93.34	63.39	-21.52	29.08	62.93	99.85
1907	115.00	115.00	-155.00	130.00	40.00	90.00
1909	110.00	0.00	-160.00	90.00	0.00	90.00
1924	-70.11	-159.89	155.00	86.47	93.53	5.00
1930	-97.18	-1.49	-18.95	81.71	55.74	144.47
1931	102.72	134.93	-165.04	104.45	16.94	98.65
1933	111.00	-152.11	-159.43	88.27	14.11	104.00
1943	139.29	-132.72	-130.36	90.84	22.54	112.52
1957	90.08	-6.22	-177.27	85.90	33.12	57.20
1963	-65.00	25.00	0.00	90.00	90.00	180.00
1971	140.00	140.00	-130.00	95.00	5.00	90.00
1978	115.11	24.89	-110.00	86.47	86.47	5.00
1986	-115.44	-24.56	-70.00	82.95	82.95	170.00
1992	-70.44	20.44	-25.00	82.95	82.95	170.00
1995	-40.00	-40.00	-130.00	45.00	135.00	90.00
2024	-155.00	115.00	0.00	90.00	90.00	0.00
2039	-53.68	50.36	-34.74	31.40	81.58	120.00
2064	105.00	0.00	-165.00	90.00	0.00	90.00
2065	48.06	-30.88	107.10	110.02	62.25	35.31
2069	95.00	95.00	-175.00	105.00	15.00	90.00
2082	125.00	125.00	-145.00	110.00	20.00	90.00
2087	100.00	100.00	-170.00	110.00	20.00	90.00
2092	80.00	80.00	170.00	125.00	35.00	90.00
2096	110.00	110.00	-160.00	105.00	15.00	90.00
2099	129.64	-126.33	-145.26	81.58	31.40	120.00
2104	117.94	31.59	-159.36	95.19	54.96	35.53
2117	39.29	127.28	129.64	90.84	22.54	112.52
2121	90.00	0.00	180.00	90.00	0.00	90.00
2123	-71.32	-175.36	89.74	31.40	81.58	60.00
2125	77.21	133.98	-178.50	114.11	39.24	118.88
2130	97.72	129.93	-170.04	104.45	16.94	98.65
2144	122.61	48.91	-164.49	107.45	48.24	46.92
2150	105.00	0.00	-165.00	90.00	0.00	90.00
2151	-53.96	28.94	-83.26	61.90	103.03	148.53
2158	60.00	60.00	150.00	120.00	30.00	90.00
2163	-20.00	-20.00	-110.00	45.00	135.00	90.00
2176	105.00	105.00	-165.00	105.00	15.00	90.00
2179	90.00	0.00	180.00	90.00	0.00	90.00
2183	-135.00	45.00	-45.00	10.00	80.00	90.00

Num.	Azimuth			Angle		
	P	T	B	P	T	B
2184	107.95	-158.54	-162.11	89.56	7.06	97.05
2188	-71.78	-158.22	155.00	76.00	104.00	20.00
2194	103.90	35.06	177.25	109.89	45.07	51.62
2204	15.00	0.00	105.00	90.00	0.00	90.00
2213	-105.00	-15.00	0.00	90.00	90.00	179.98
2218	-119.11	159.11	110.00	69.30	110.70	30.00
2223	-50.00	-140.00	0.00	90.00	90.00	0.00
2228	-114.07	-29.89	-123.43	38.13	94.56	127.76
2233	-60.00	-150.00	0.00	90.00	90.00	0.00
2240	-95.68	-174.32	135.00	66.07	113.93	35.00
2249	-102.82	-1.47	-81.93	43.50	79.42	131.56
2257	-65.38	10.90	-91.12	44.63	103.18	131.64
2258	-65.00	-65.00	-155.00	45.00	135.00	90.00
2262	150.00	-30.00	-120.00	85.00	5.00	90.00
2267	0.00	0.00	-90.00	0.00	90.00	90.00
2270	97.21	153.98	-158.50	114.11	39.24	118.88
2272	-90.00	-90.00	-180.00	45.00	135.00	90.00
2281	-45.00	-135.00	0.00	90.00	90.00	0.00
2282	103.95	174.11	-161.10	100.18	27.89	115.66
2283	75.89	146.05	51.10	27.89	100.18	115.66
2290	-79.59	7.83	-84.21	41.65	92.30	131.56
2301	94.29	-177.72	-175.36	90.84	22.54	112.52
2305	40.00	40.00	-50.00	15.00	105.00	90.00
2325	-135.00	-135.00	135.00	45.00	135.00	90.00
2330	105.00	105.00	-165.00	105.00	15.00	90.00
2335	-69.11	-150.89	160.00	69.30	110.70	30.00
2343	-98.20	11.12	-50.55	55.58	64.23	134.51
2357	95.88	115.80	-165.88	129.20	40.94	99.96
2375	160.00	-20.00	-110.00	85.00	5.00	90.00
2381	91.53	120.84	-166.34	128.23	42.09	104.94
2386	110.40	120.47	-155.44	129.80	40.24	94.98
2399	128.47	99.16	-153.66	128.23	42.09	75.06
2411	92.92	-137.27	-177.69	84.60	8.39	96.41
2413	-148.43	158.43	95.00	52.24	127.76	60.00
2416	-70.78	22.59	-10.65	79.40	72.56	159.41
2417	95.88	115.80	-165.88	129.20	40.94	99.96
2420	55.88	75.80	154.12	129.20	40.94	99.96
2437	73.01	-25.27	167.45	83.90	36.61	54.07
2450	107.92	-122.27	-162.69	84.60	8.39	96.41
2451	80.00	-100.00	170.00	75.00	15.00	90.00
2452	-111.63	163.74	104.41	68.94	103.65	25.46
2466	107.48	80.49	-165.74	109.41	21.57	80.95
2469	107.95	-158.54	-162.11	89.56	7.06	97.05
2470	-102.94	166.92	75.99	68.91	89.64	21.09
2488	90.79	49.67	170.38	117.31	34.43	70.71
2514	-55.00	-145.00	0.00	90.00	90.00	0.02
2526	90.00	90.00	180.00	105.00	15.00	90.00
2536	180.00	-180.00	90.00	35.00	125.00	90.00
2544	78.15	21.07	161.15	106.38	28.40	67.48
2545	115.00	-65.00	-155.00	85.00	5.00	90.00
2547	-70.00	-160.00	0.00	90.00	90.00	0.00

Figure Captions

1) Isoseismal maps for Weber I and II. Individual observations are indicated by a numeral giving the modified Mercalli intensity. A: Weber I; B: Weber II.

2) The south-east of North Island, New Zealand. The Pacific and Australian plates are converging in a direction of about 80-260 degrees, with a rate of about 5 cm/yr. The solid circles are the closer permanent stations of the National Seismograph Network. More distant stations, used for locations only if fewer than 6 closer stations, permanent or temporary, are available, are indicated by open circles.

3) The Weber region. The four main-shocks are indicated by circles; an event in 1975, magnitude 5.7, depth 57 km, is indicated by a small circle. The portable stations (not all occupied at the same time - see Table 1) and the closest permanent station (PGZ) are shown by triangles. The major Mohaka-Ruahine fault zone is in the northwest of the region; the Waewaepa-Mangatoro-Oruawhara shear zone is towards the centre. The box indicates the area used for detailed studies of the aftershocks.

4) Hypocentres of all relocated events, January 1989 - March 1992, qualities A, B, C, and D. The coordinate centre is at 40.315 S, 176.325 E; the X axis strikes N45E; Y strikes N45W. A: Map view; B: projected onto the X plane; C: projected onto the Y plane.

5) Quality A hypocentres. The coordinate centre is at 40.315 S, 176.325 E. As discussed in the text, the X axis for shallower events strikes N35E; for deeper events it strikes N50E. The hypocentres of Weber I and II are shown by open circles although their qualities are only C and D respectively. A: map view; B: projected onto the X plane; C: projected onto the Y plane.

6) The envelope of quality A hypocentres projected onto the X plane (as in Figure 5b) for Weber I and II; quality A and B for Weber III and IV. A projection onto the perpendicular Y plane indicates that the deep aftershock zones are nearly coplanar. Circles are hypocentres of the main shocks.

7) Magnitude-time history of the Weber sequence, January 1989 - March 1992, qualities A-D. Events with depths more or less than 19 km are shown separately.

8) Frequency - Magnitude plots; N is the cumulative number. A: Depth ≥19 km. The b-value is determined by the maximum likelihood method. The short vertical line represents the adopted magnitude threshold. B: Depth <19 km. Because of the non-linearity no b-value is calculated.

9) Aftershock rate as a function of time, for events of magnitude 2.65 or more. A: Weber I, III, and IV (using the time of Weber I as the origin); B: Weber II. A least squares fit of a line is shown, points corresponding to the dashed regions not being used in the fit.

10) Focal mechanism solutions, lower hemisphere. The solid nodal planes are the best fitting double-couple to centroid moment tensor solutions (see text for references). The dashed planes are solutions modified to better fit the first motion data. Teleseismic first motion data are from the US Department of the Interior (1990a,b), iP only, distance 96 degrees or less, incidence angles from Pho & Behe (1972). Local first motion data have been corrected for known polarity reversals. P and T are the principal axes for the solid planes; P' and T' are for the dashed planes. A: Weber I; B: Weber II.

11) Lower hemisphere plots of the P and T axes of aftershock mechanisms. Open circles are the T axes, solid circles are the P axes. A: Weber I aftershocks; B: Weber II aftershocks.

12) Time variation of the difference between the observed and expected cumulative number of Weber I aftershocks (see text). Day 0 is January 1 1989. The times of Weber I and II are indicated by vertical lines. Only events of magnitude 2.65 or more are used. The initial large offset is due to the missing of many very early aftershocks (in the first few hours) and to extrapolation of equation (3) to very small times.

13) Time variation in mean magnitude for the Weber I aftershocks. Day 0 is January 1, 1989. Only events of magnitude 2.65 or more are used. Each point is an average for the preceding 25 events. The times of Weber I and II are indicated by vertical lines. Error bars (+ or - one standard error of the mean) for independent points are shown by short vertical lines.

14) A: Hypocentres of quality A events projected onto the Y plane (see Figure 5a for a full explanation), plus an interpretation of the velocity model and focal mechanism results. B: Cartoon (with greatly exaggerated and generalized topography, etc) model of the southeast coast of the North Island.

(1A)

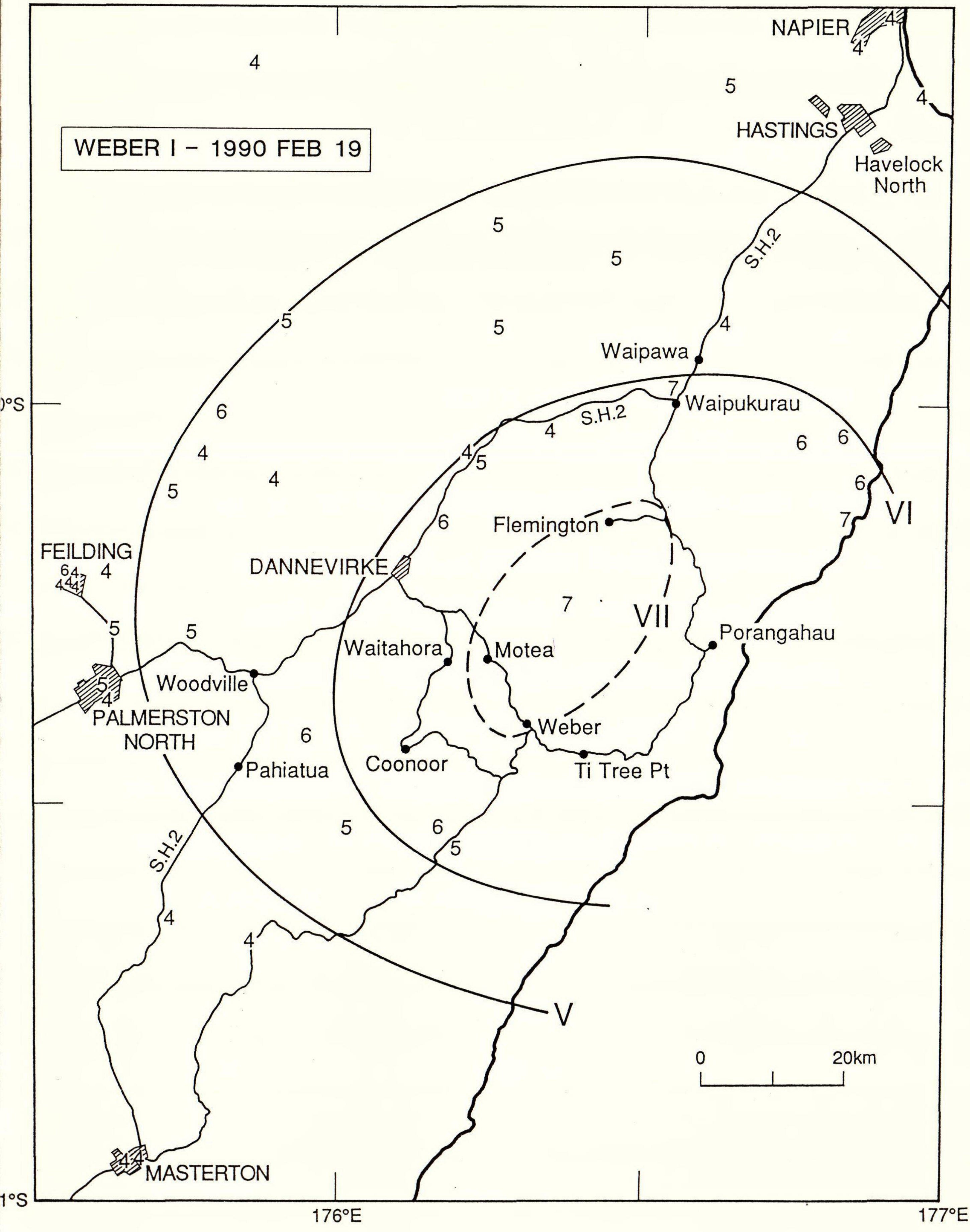
WEBER I - 1990 FEB 19
NAPIER
HASTINGS
Havelock North
S.H.2
Waipawa
Waipukurau
FEILDING
DANNEVIRKE
Flemington
VII
VI
V
Porangahau
Waitahora
Motea
Woodville
PALMERSTON NORTH
Weber
Coonoor
Ti Tree Pt
Pahiatua
MASTERTON
0
20km
176°E
177°E

13

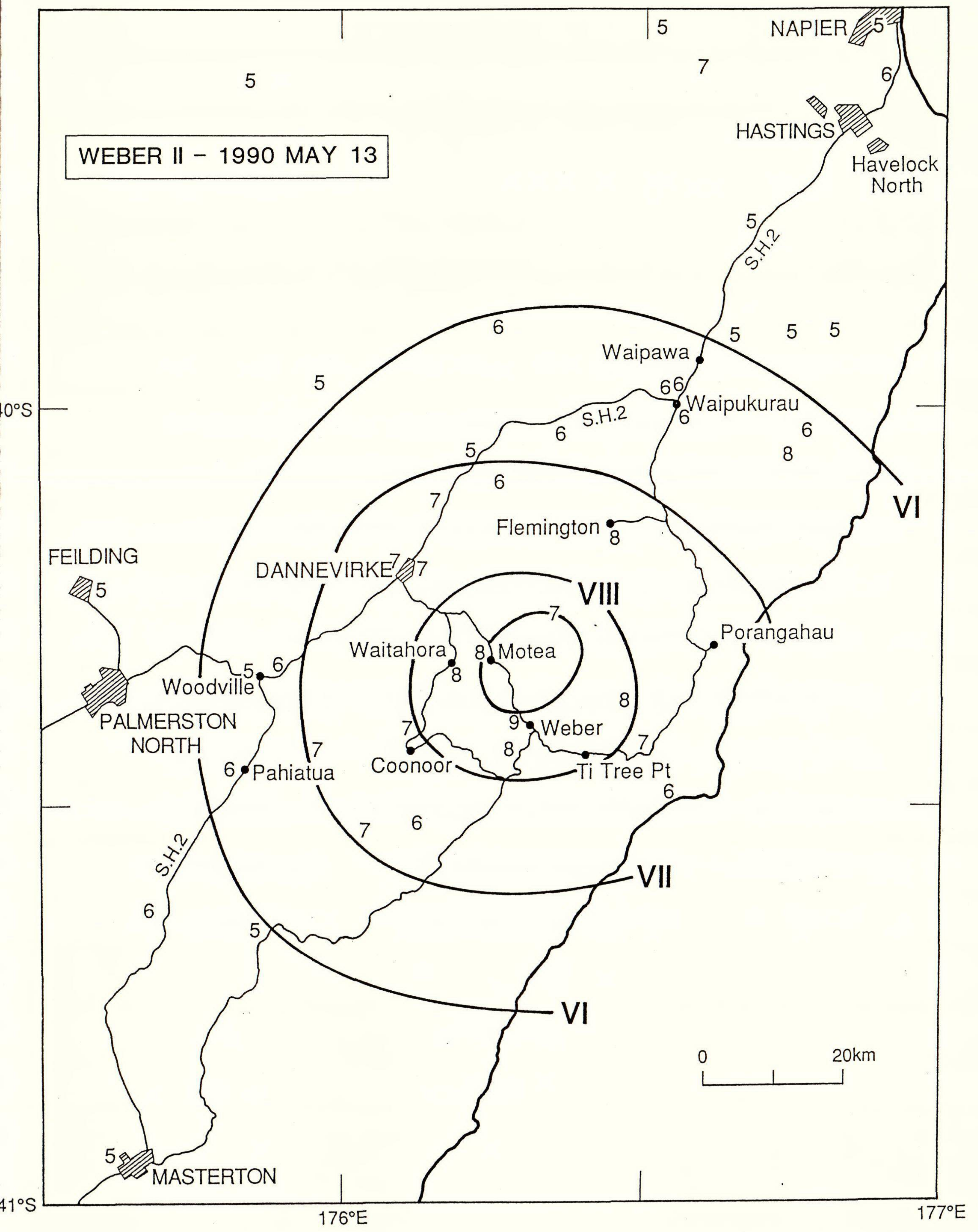
WEBER II - 1990 MAY 13
NAPIER
HASTINGS
Havelock North
S.H.2
Waipawa
Waipukurau
Flemington
FEILDING
DANNEVIRKE
Porangahau
Waitahora
Motea
Woodville
PALMERSTON NORTH
Weber
Coonoor
Ti Tree Pt
Pahiatua
MASTERTON
VI
VII
VIII
0
20km
40°S
41°S
176°E
177°E

(2)

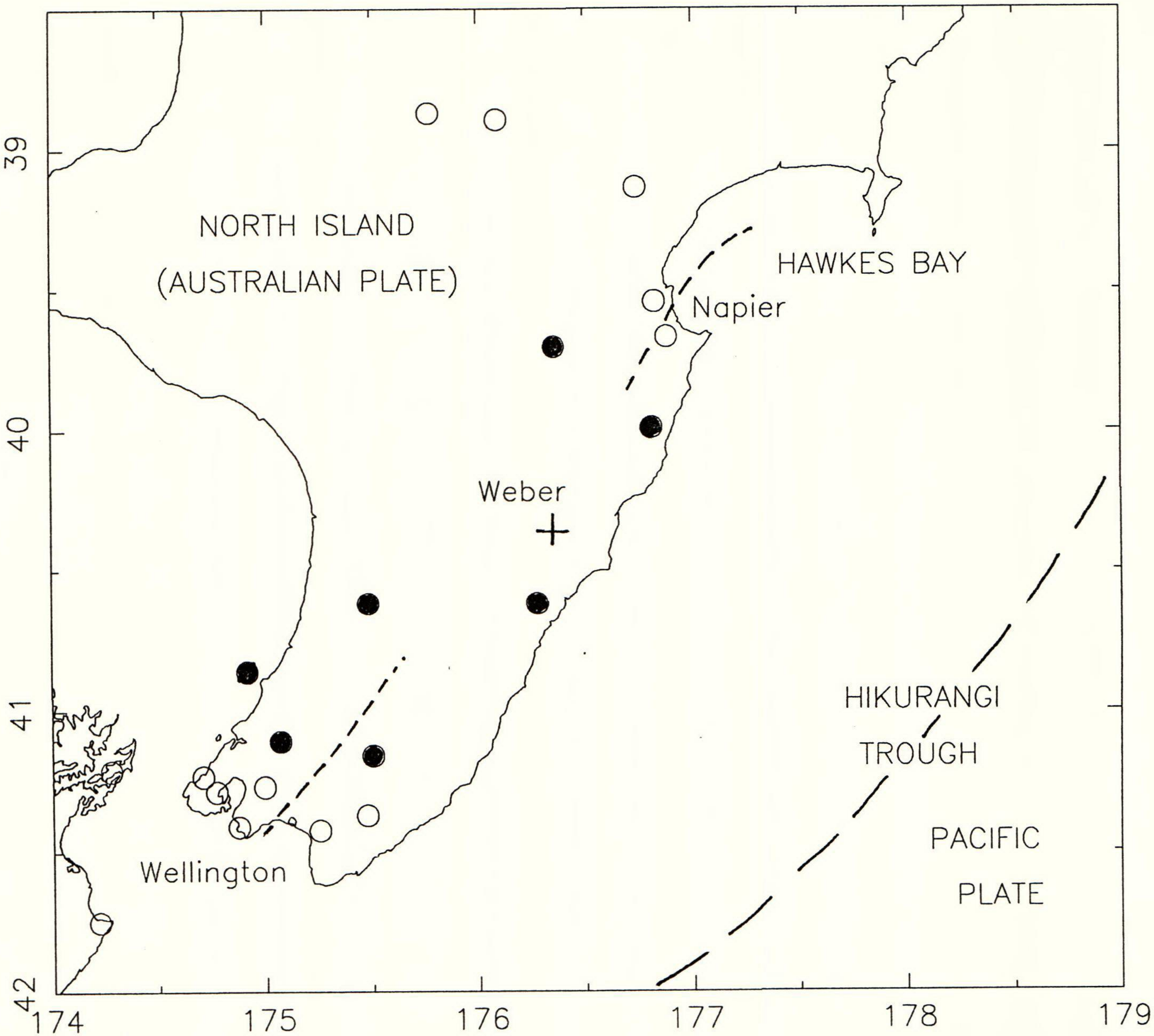
NORTH ISLAND
(AUSTRALIAN PLATE)
HAWKES BAY
Napier
Weber
Wellington
HIKURANGI
TROUGH
PACIFIC
PLATE
39
40
41
42
174
175
176
177
178
179

(3)

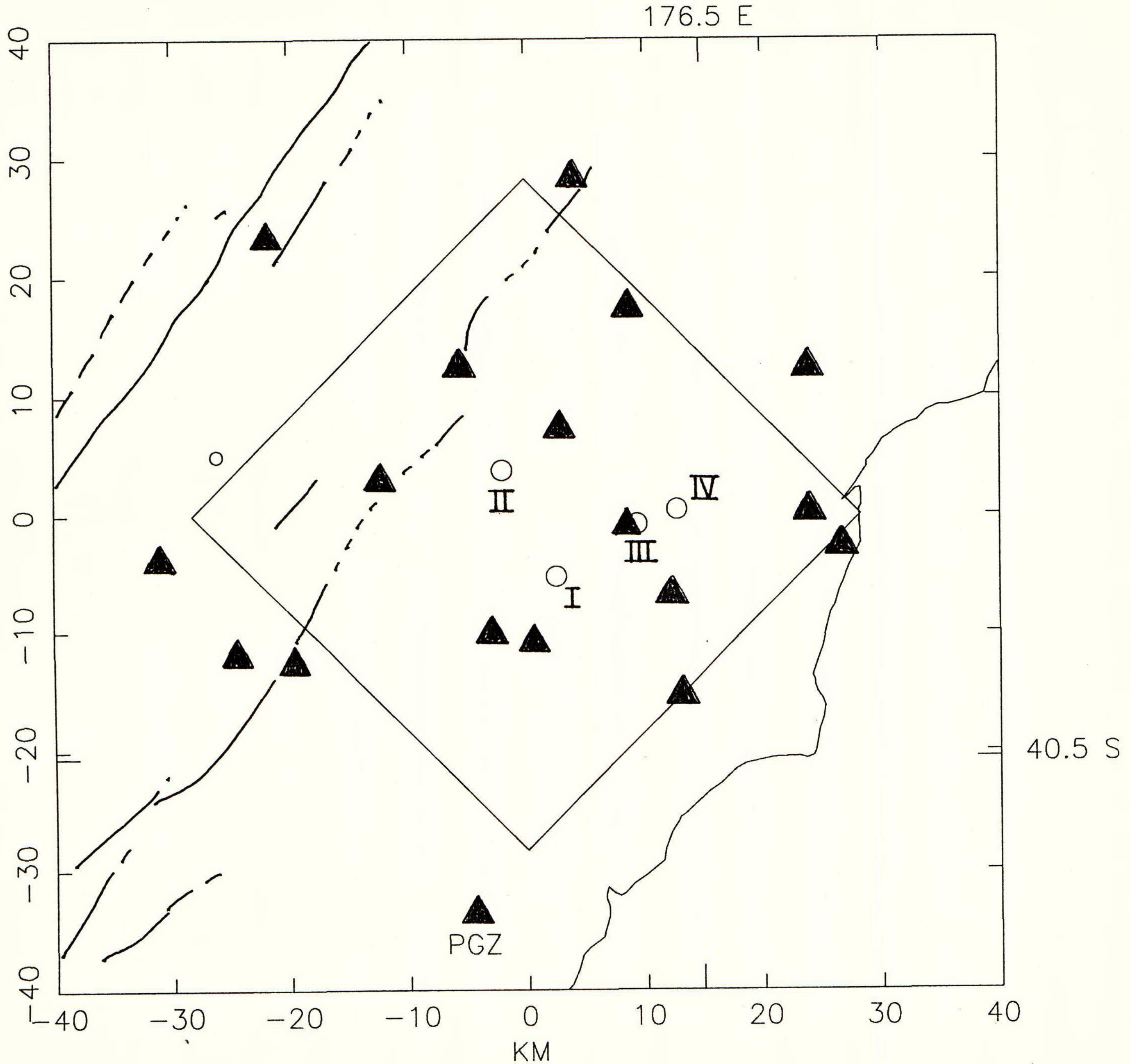

(4A)

QUALITY=ABCD, 1989–1992

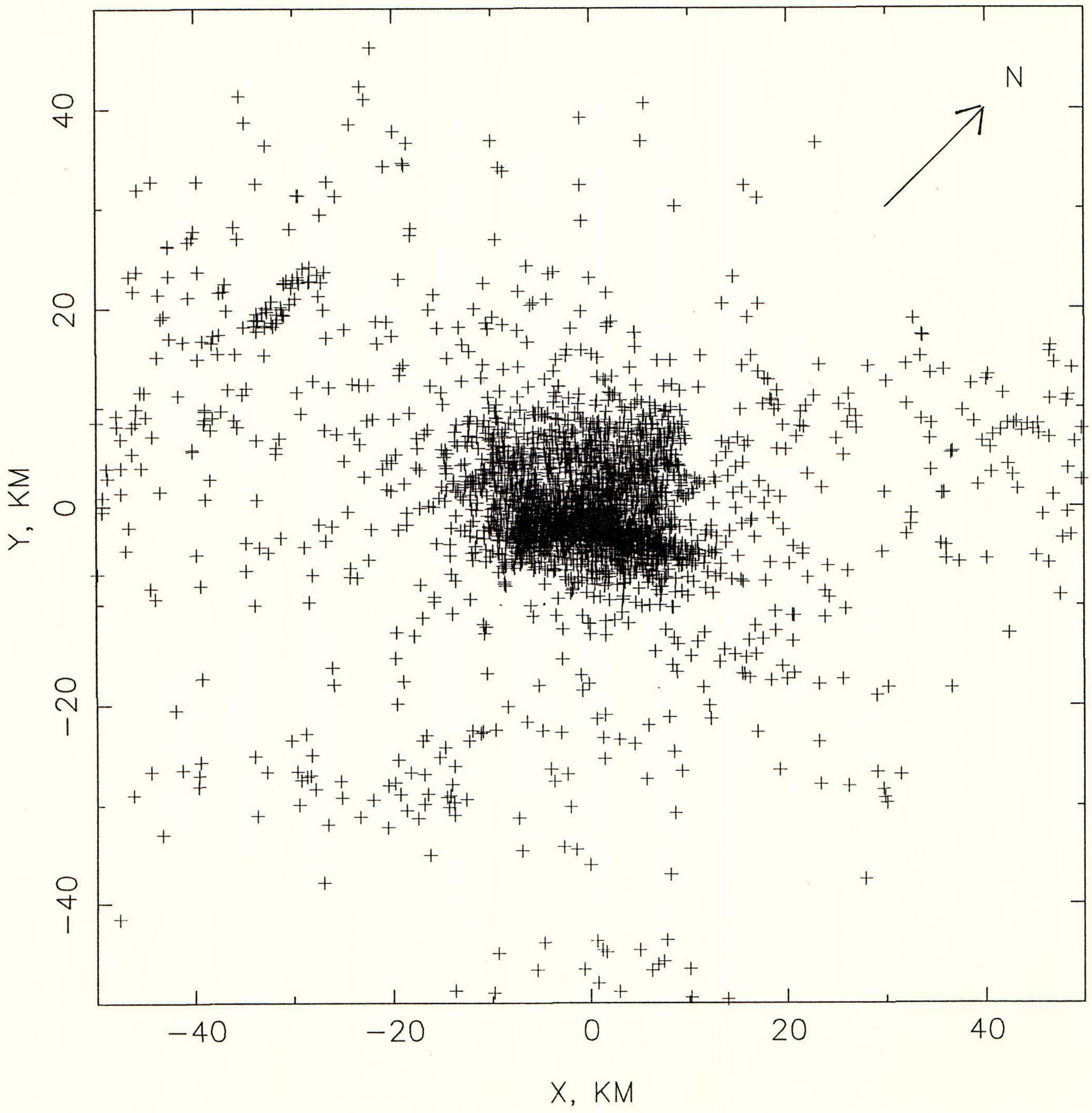

4B

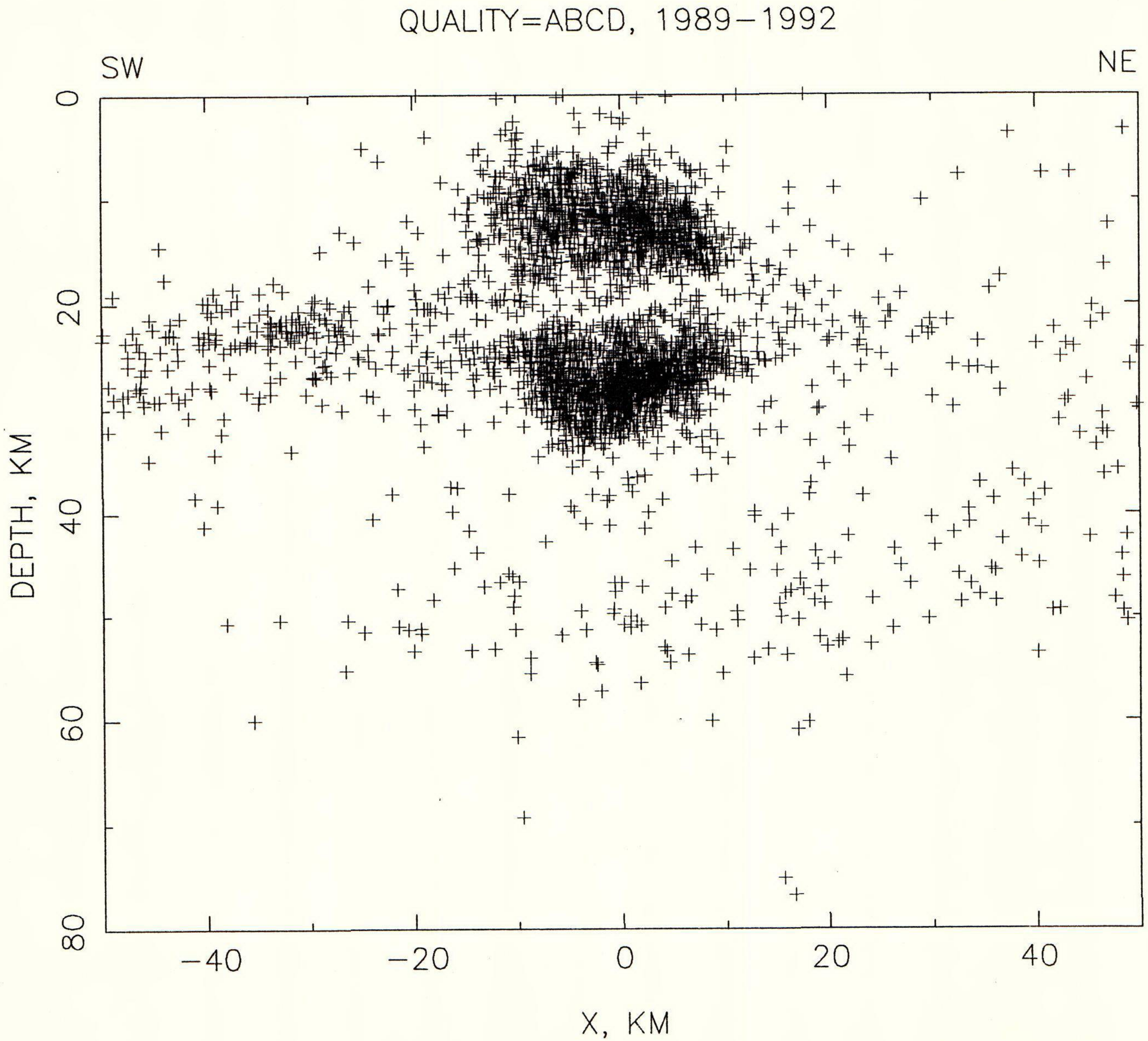

QUALITY=ABCD, 1989–1992
SW
NE
DEPTH, KM
X, KM
0
20
40
60
80
−40
−20
0
20
40

4c

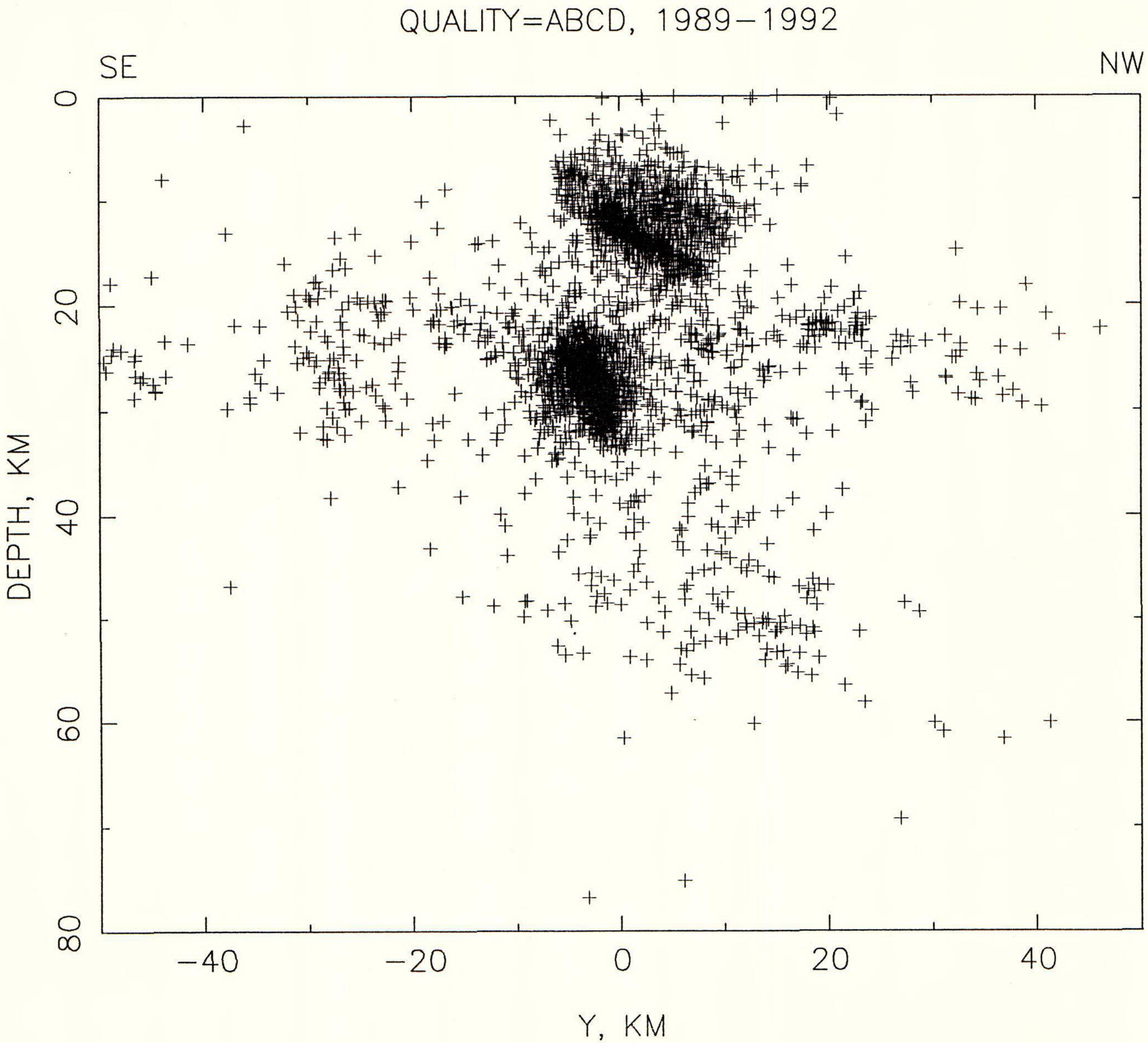
QUALITY=ABCD, 1989-1992
SE
NW
DEPTH, KM
0
20
40
60
80
-40
-20
0
20
40
Y, KM

(5A)

QUALITY=A, WEBER I & II, ROTATION=+10/-5

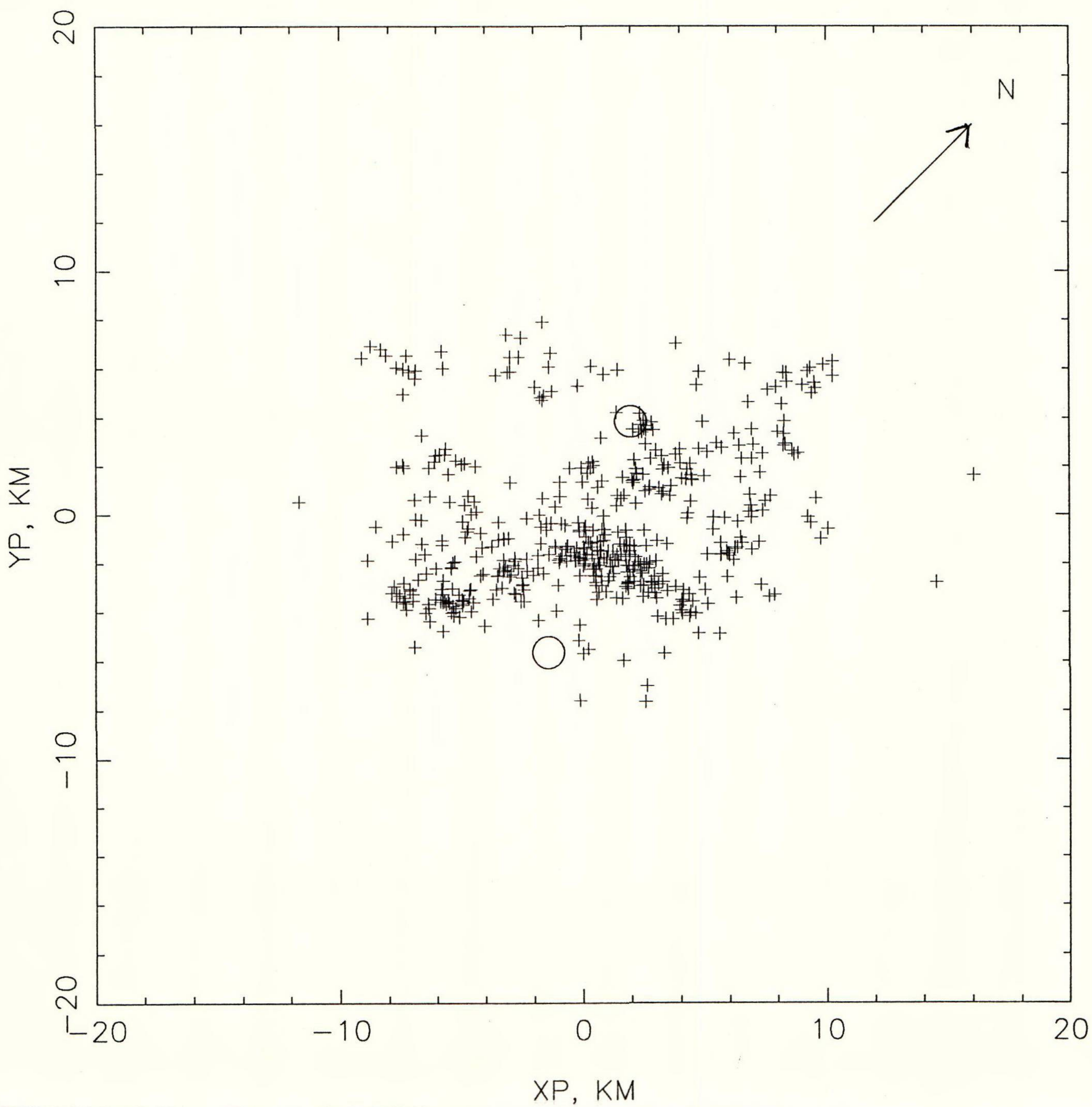

5B

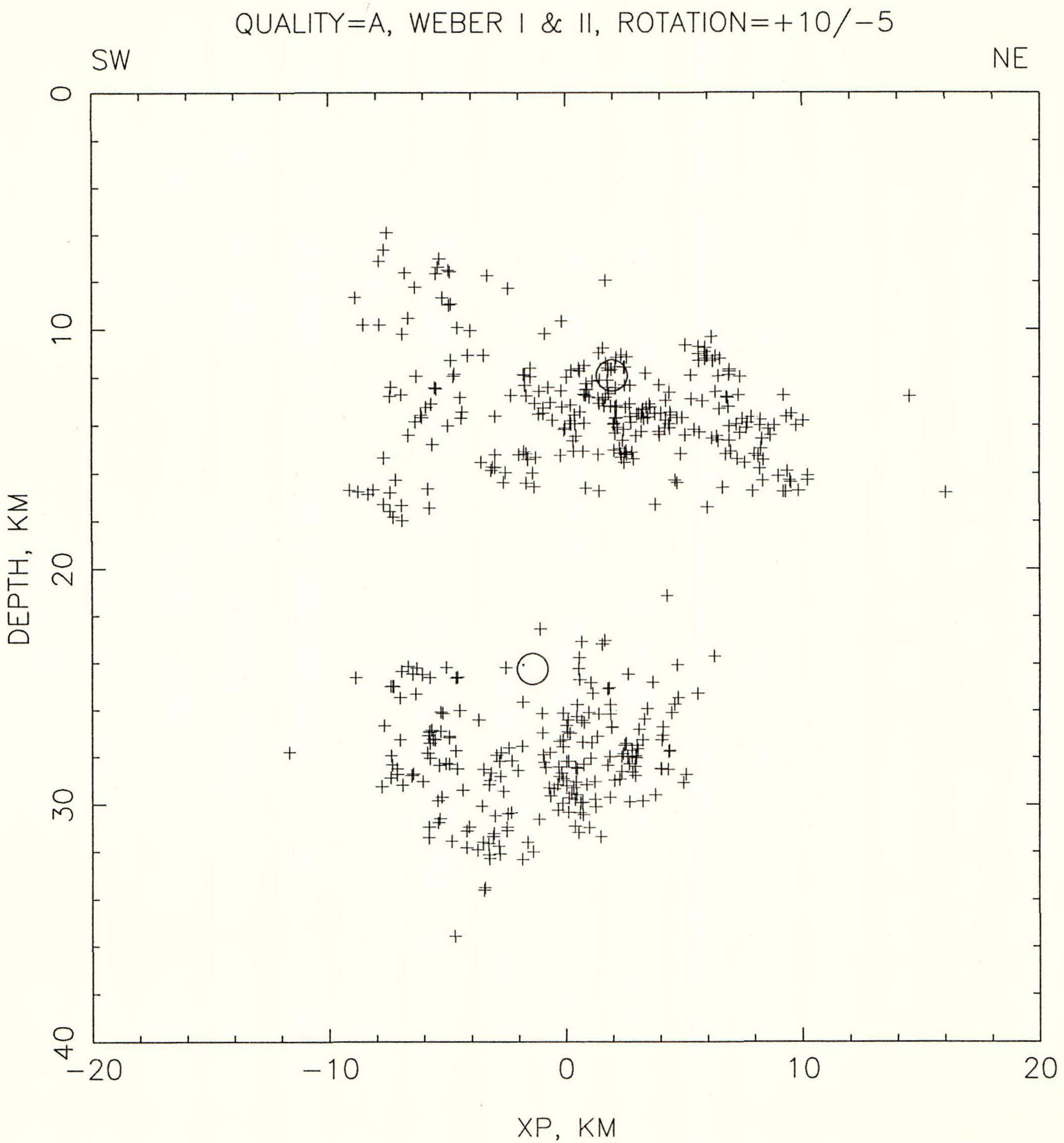
QUALITY=A, WEBER I & II, ROTATION=+10/-5
SW
NE
DEPTH, KM
XP, KM
0
10
20
30
40
-20
-10
0
10
20

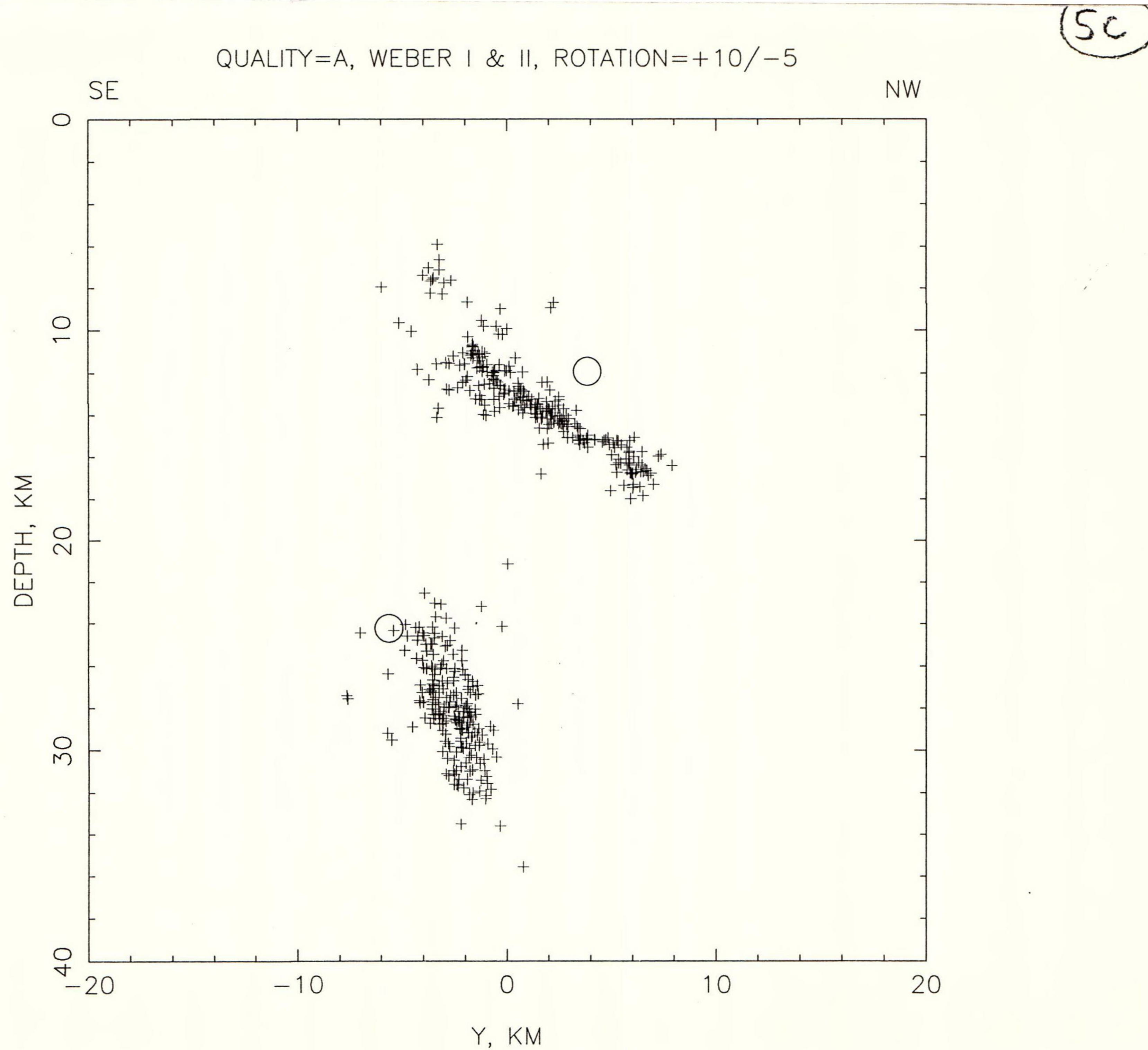

(5c)
QUALITY=A, WEBER I & II, ROTATION=+10/-5
SE
NW
DEPTH, KM
0
10
20
30
40
-20
-10
0
10
20
Y, KM

6

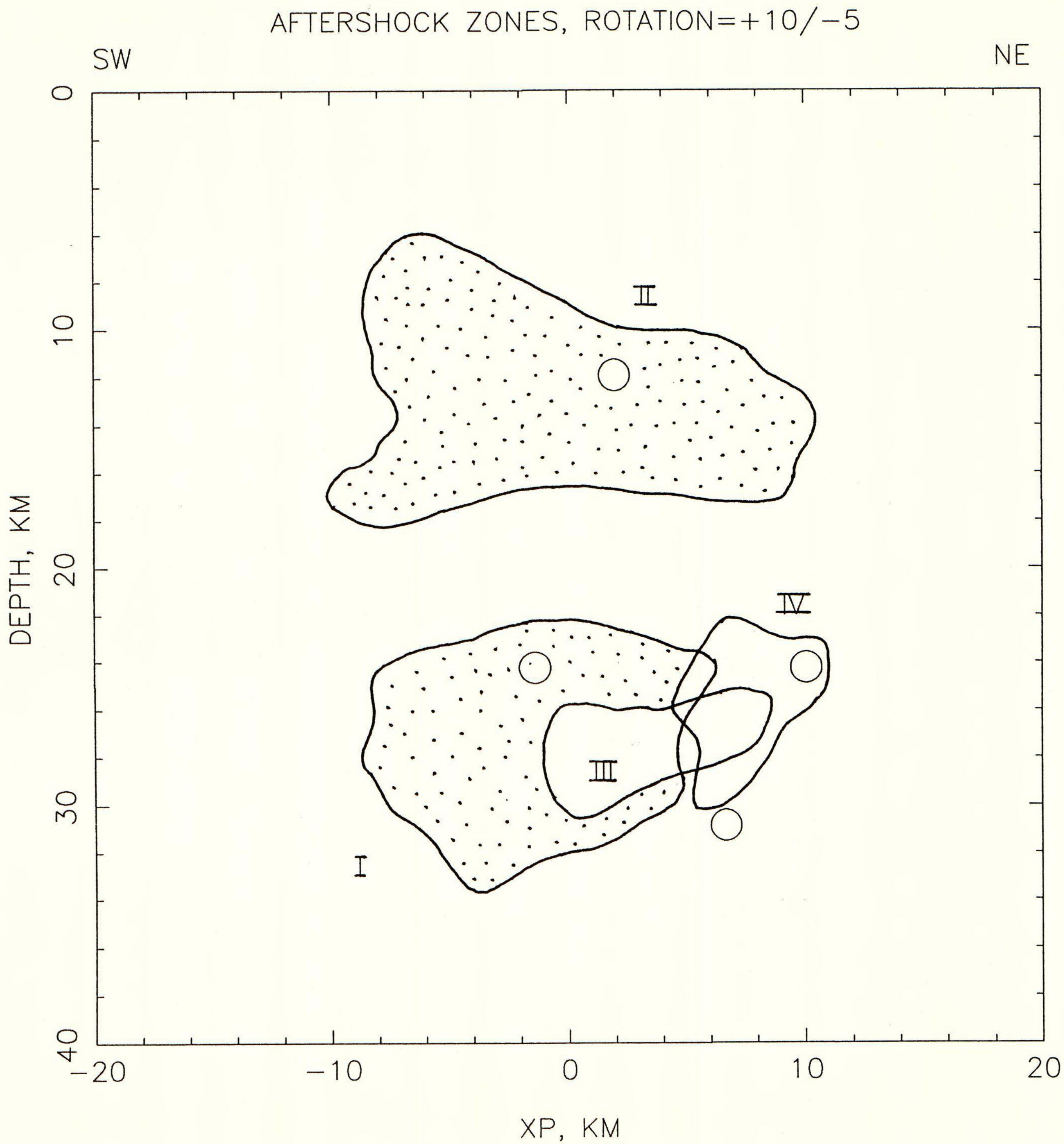
AFTERSHOCK ZONES, ROTATION=+10/-5
SW
NE
DEPTH, KM
0
10
20
30
40
XP, KM
-20
-10
0
10
20
I
II
III
IV

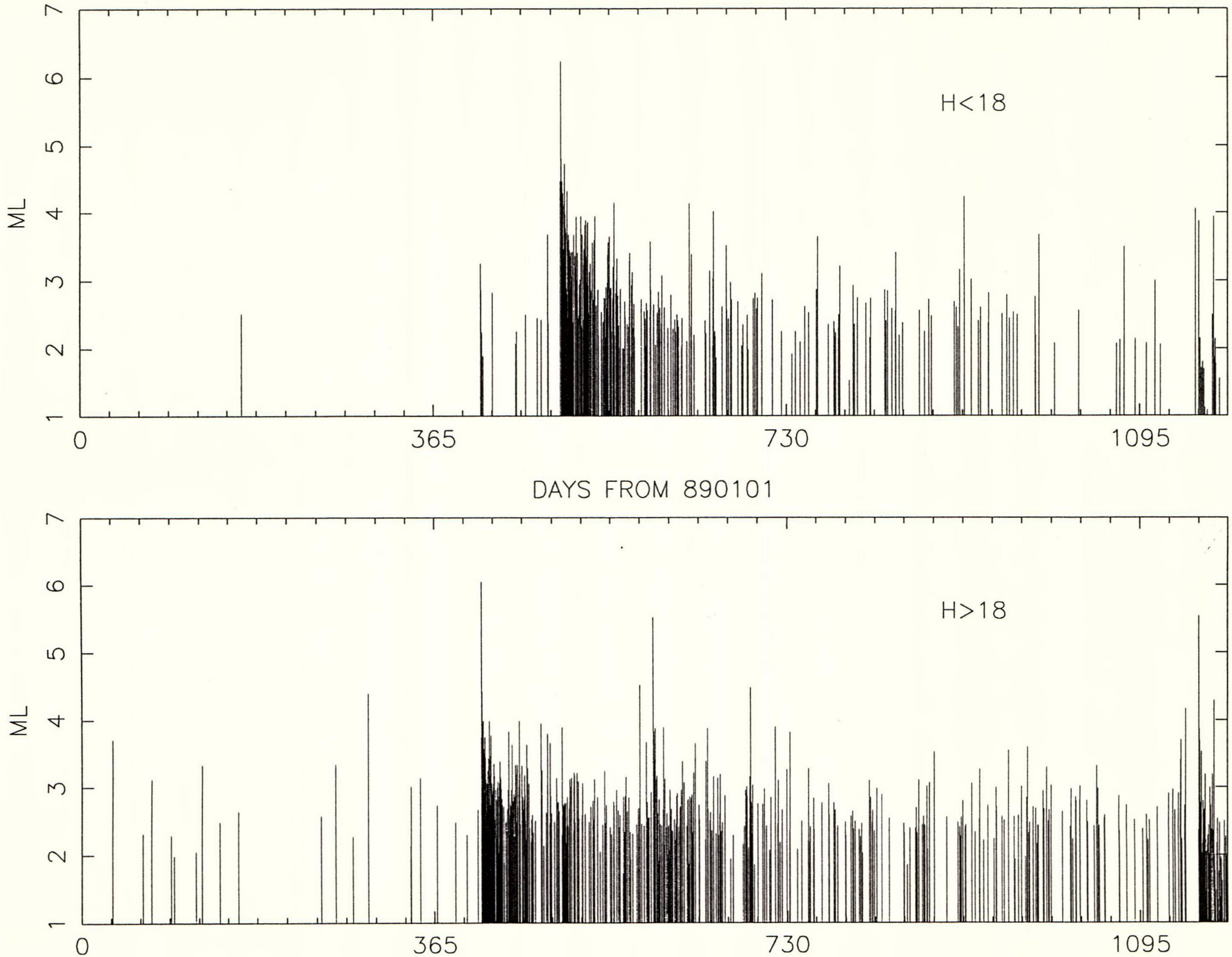
H<18
ML
DAYS FROM 890101
H>18
ML
0
365
730
1095

8A

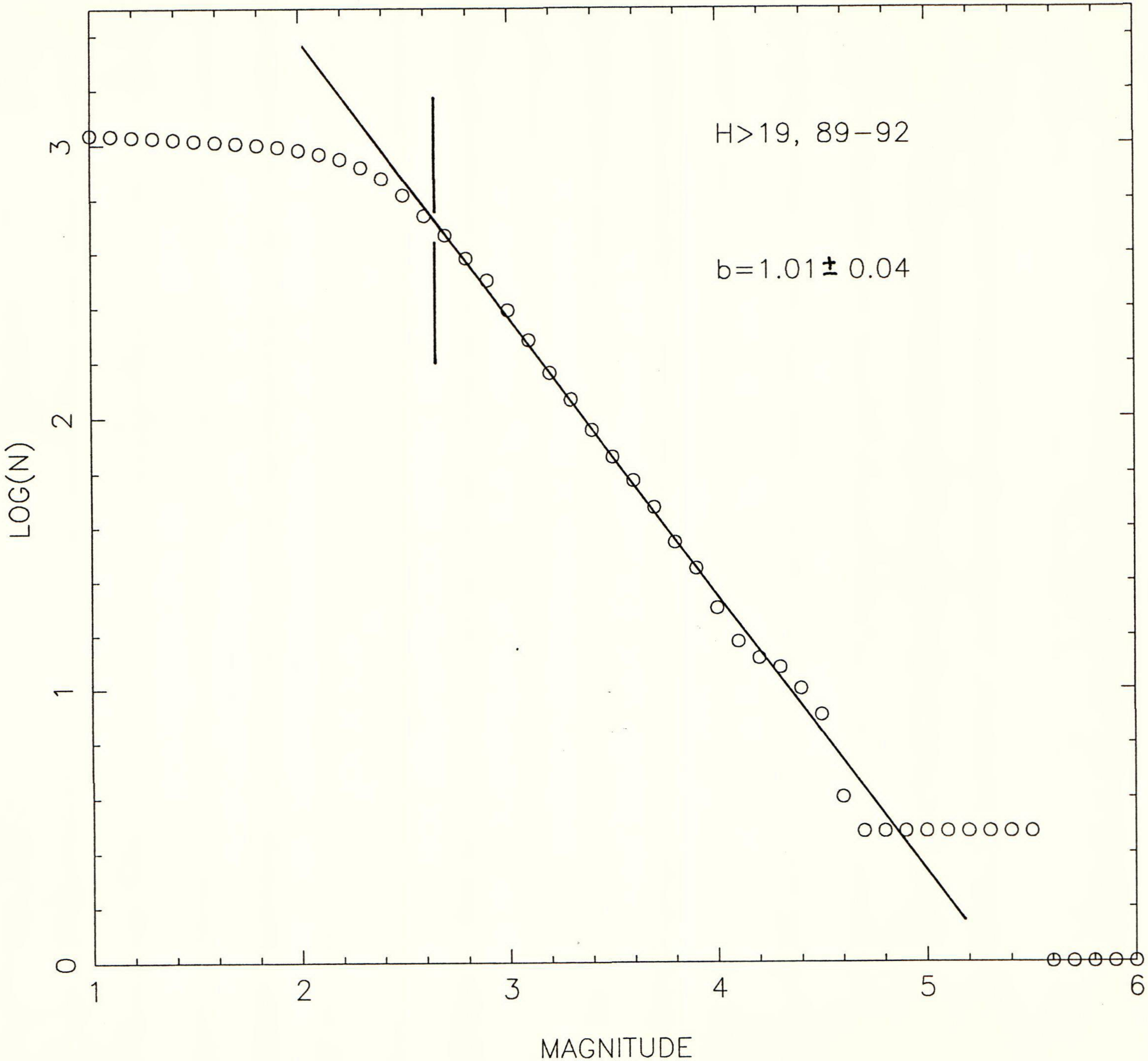

(γB)

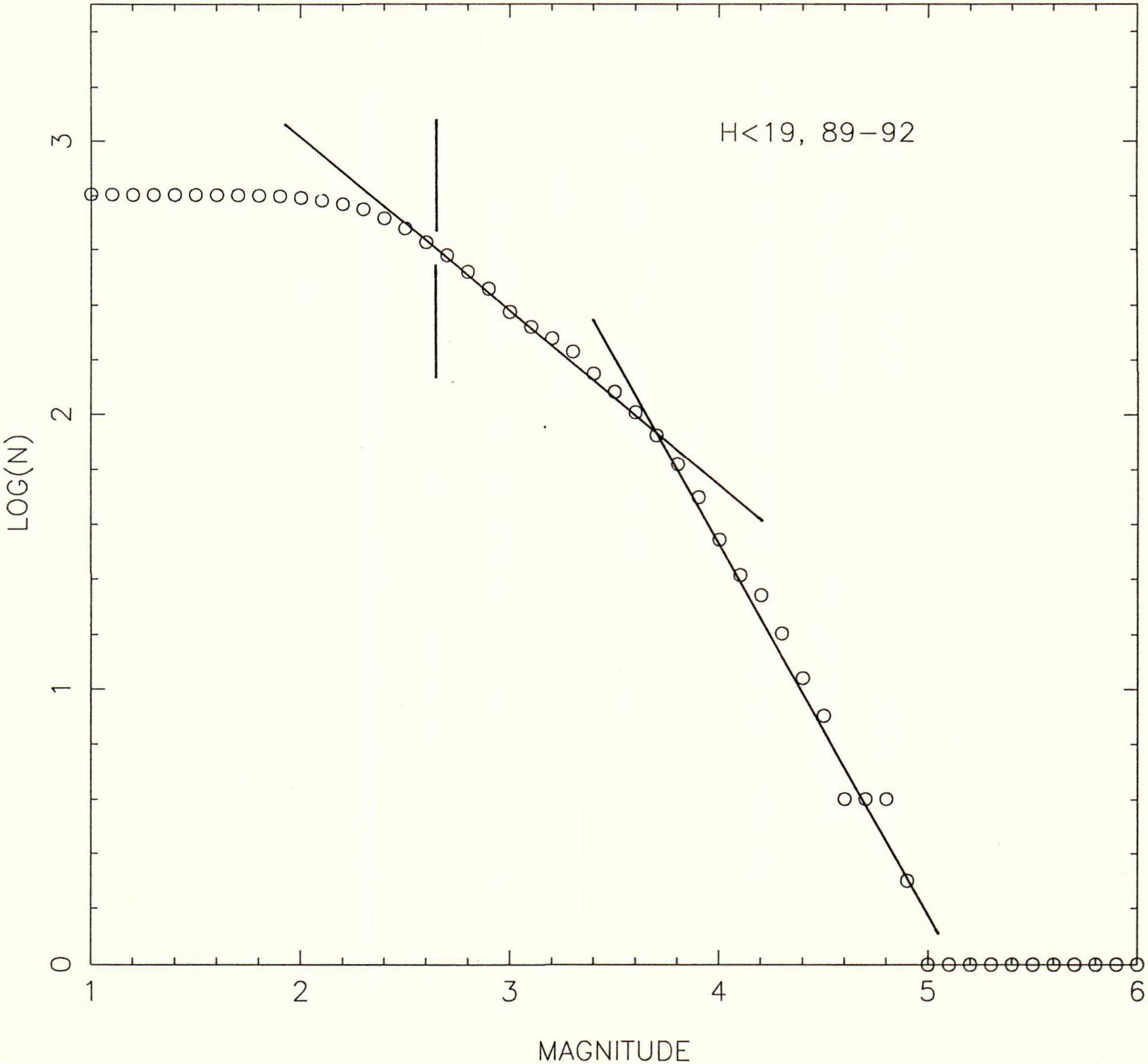

WEBER I

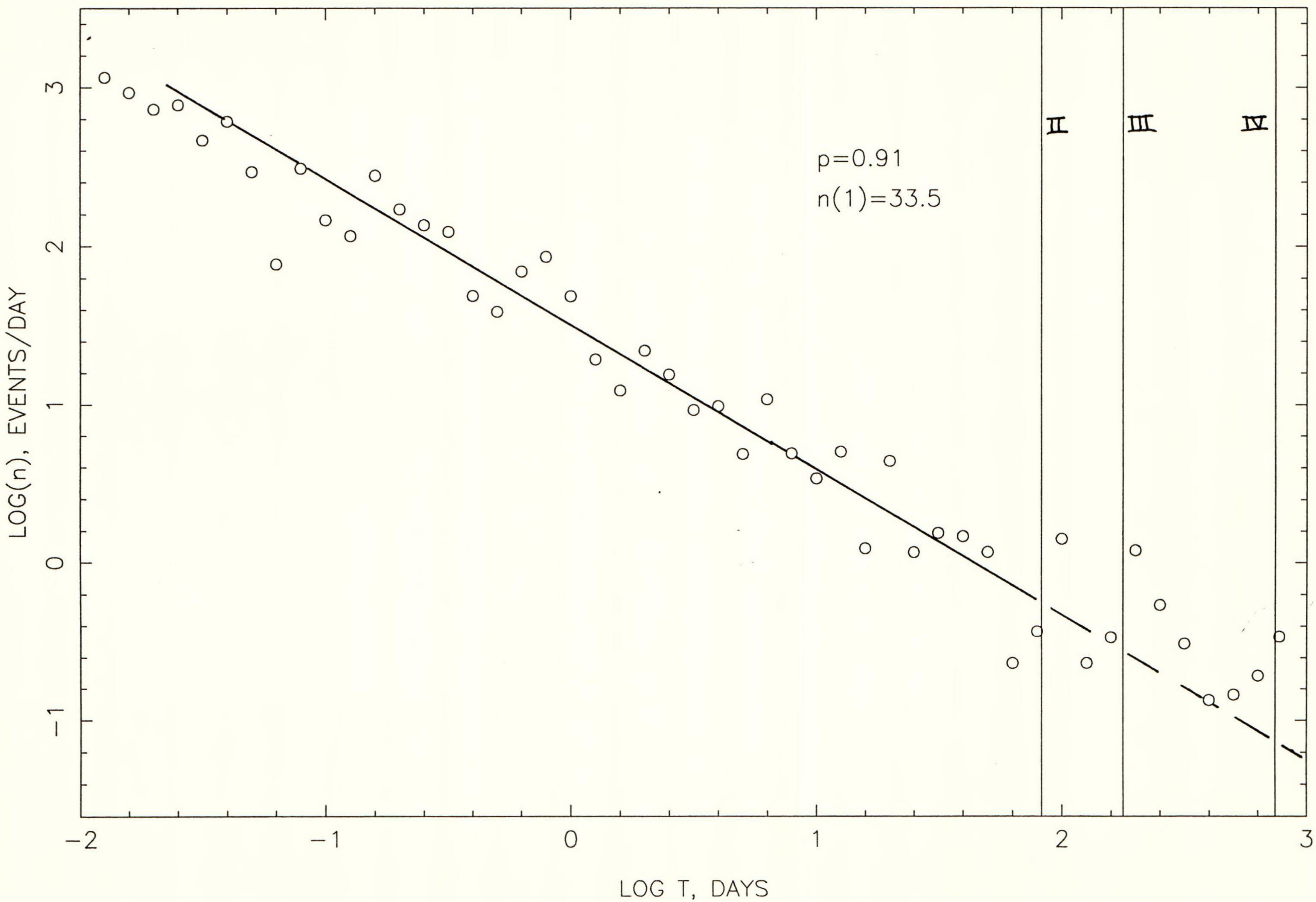

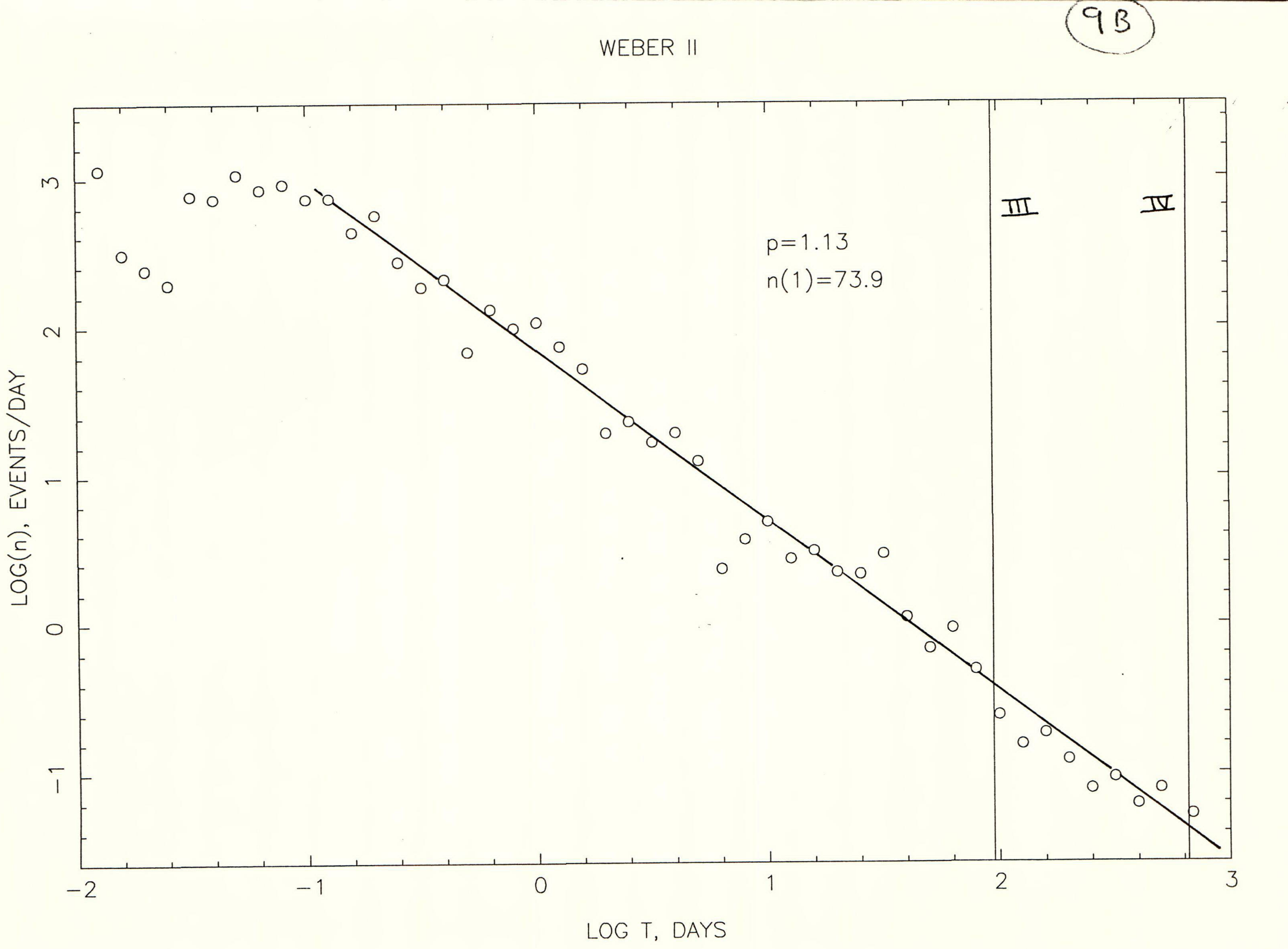

9B
WEBER II
p=1.13
n(1)=73.9
III
IV
LOG(n), EVENTS/DAY
LOG T, DAYS
−2
−1
0
1
2
3

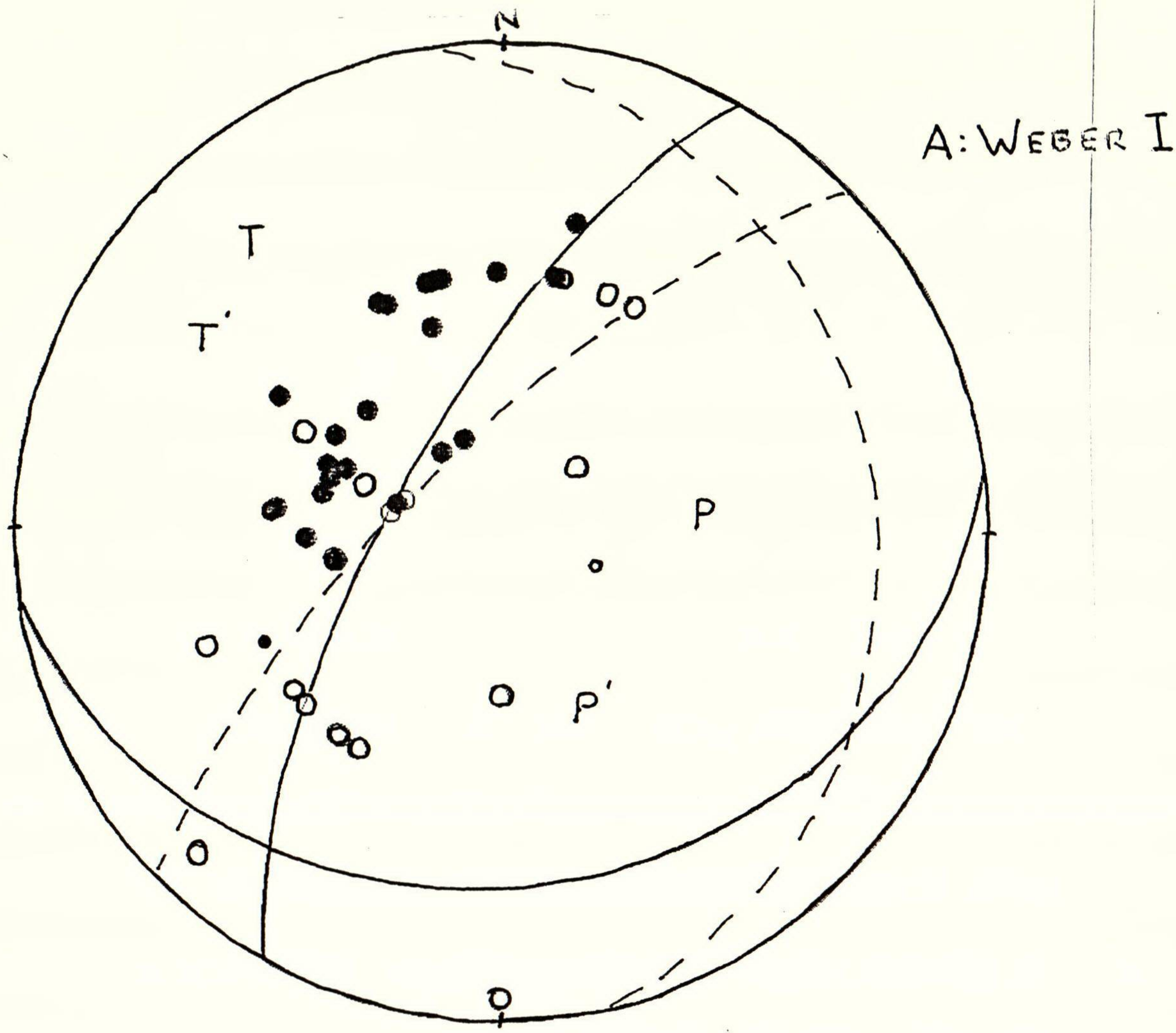
N
A: WEBER I
T
T'
P
P'

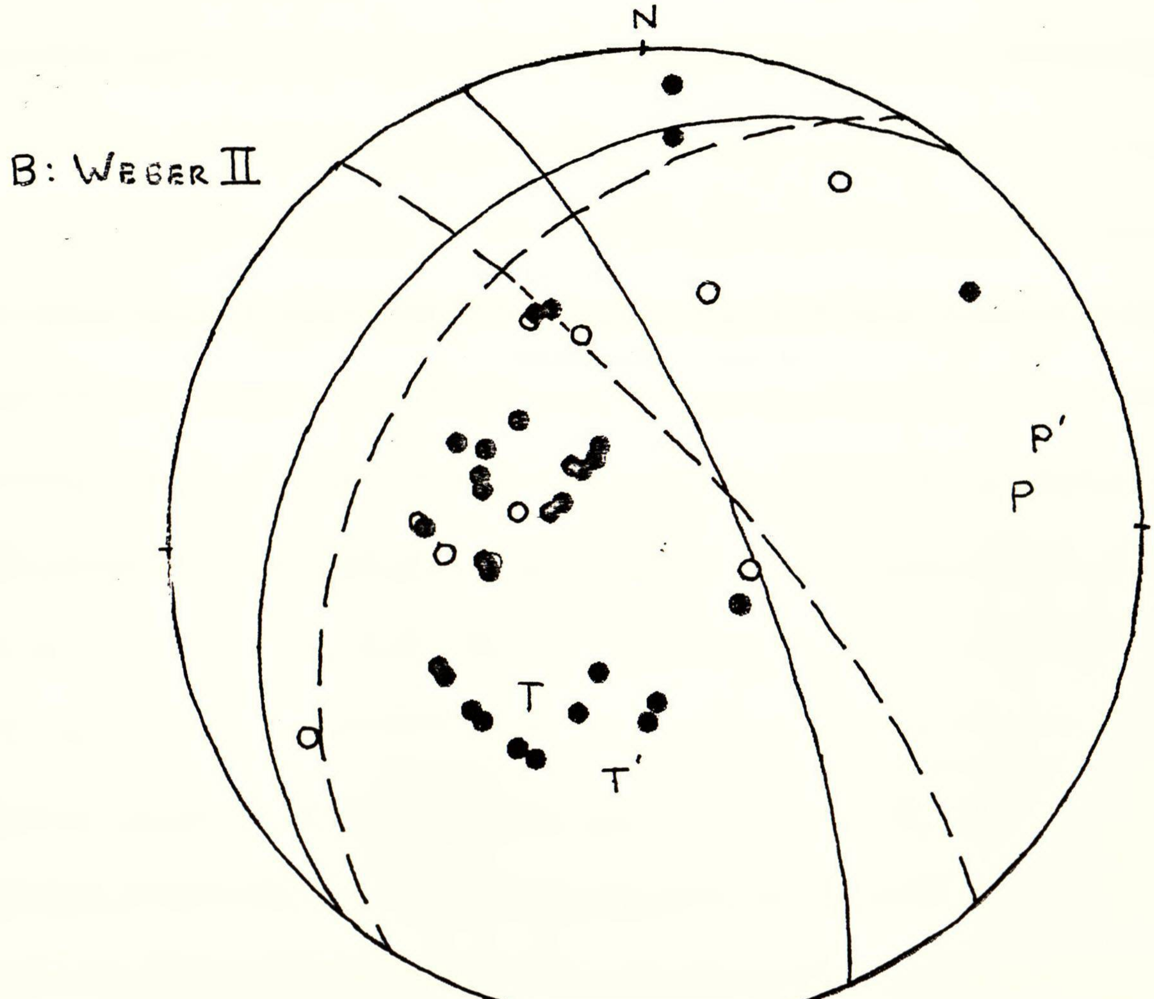
N
B: WEBER II
P'
P
T
T'

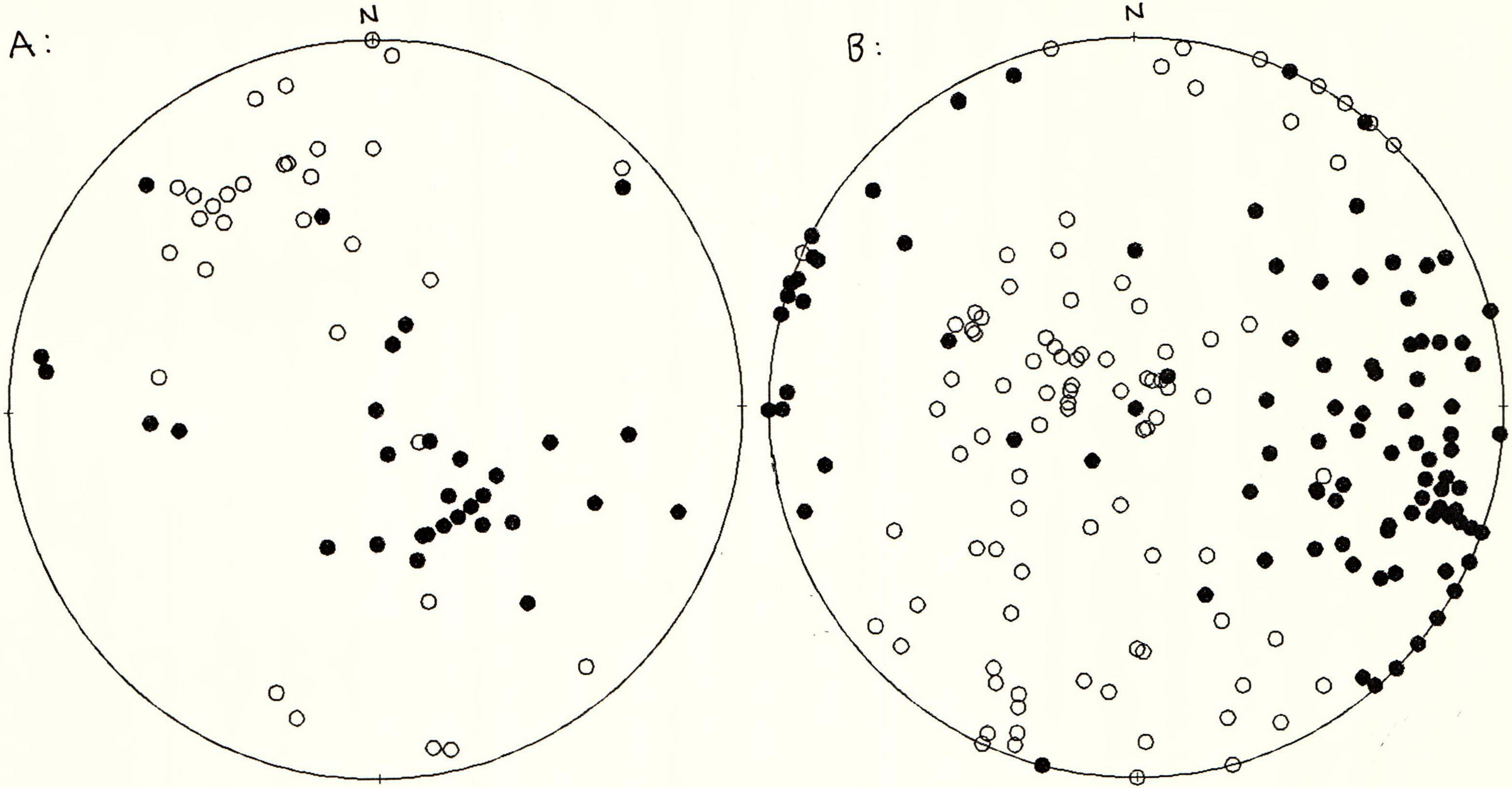
A:
N
B:
N

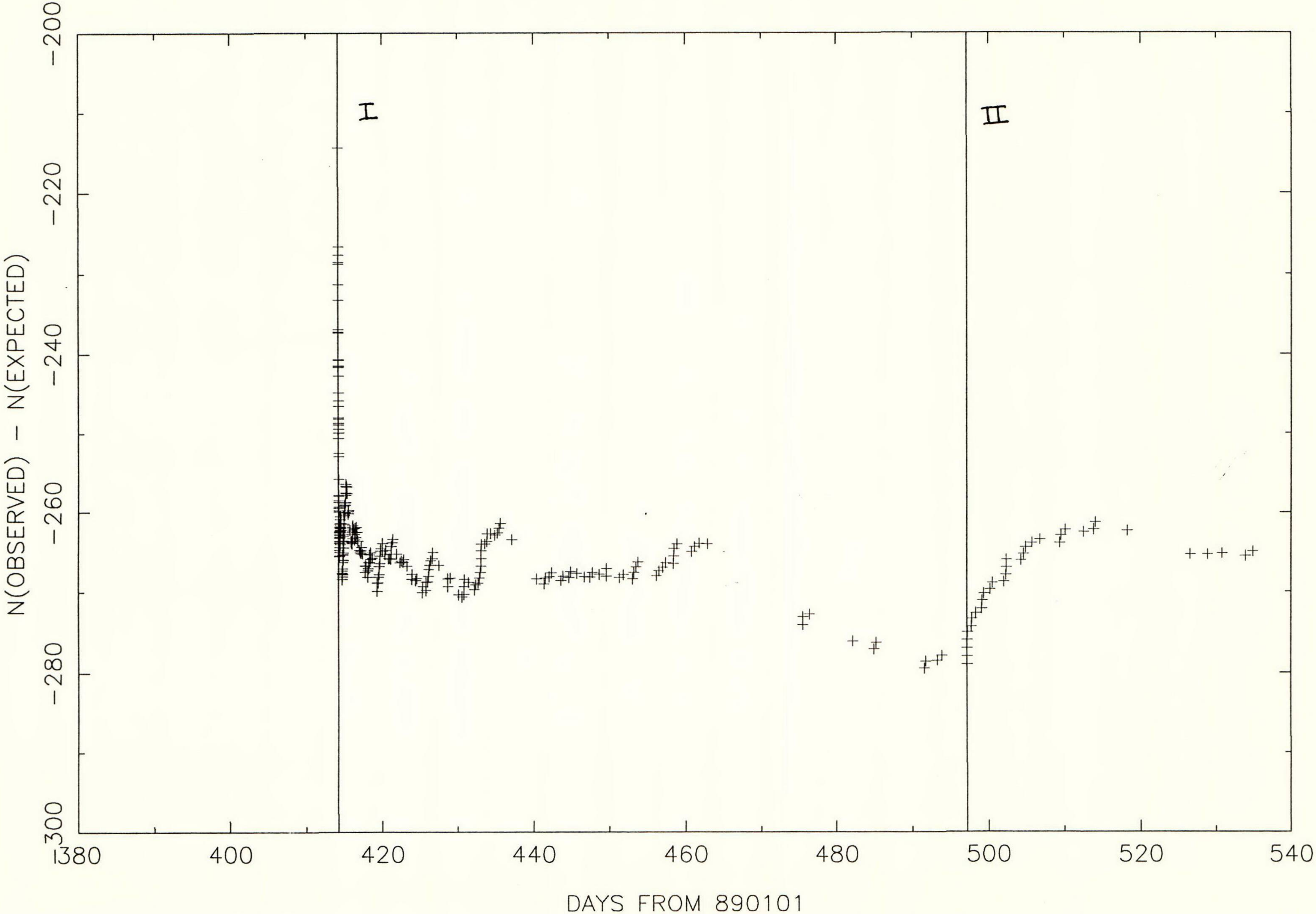
N(OBSERVED) - N(EXPECTED)
DAYS FROM 890101
I
II
-200
-220
-240
-260
-280
-300
380
400
420
440
460
480
500
520
540

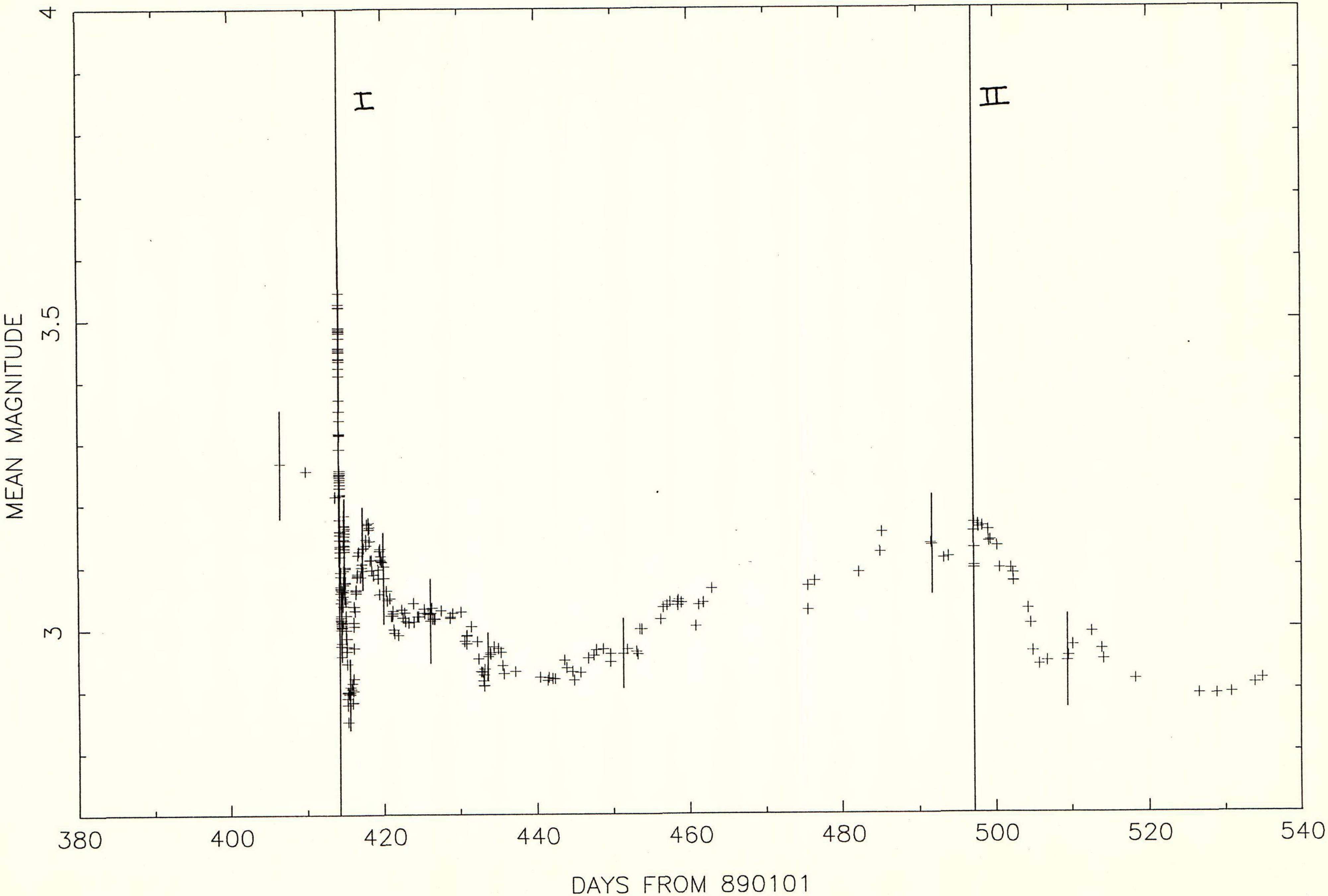

I
II
MEAN MAGNITUDE
4
3.5
3
380
400
420
440
460
480
500
520
540
DAYS FROM 890101

14A

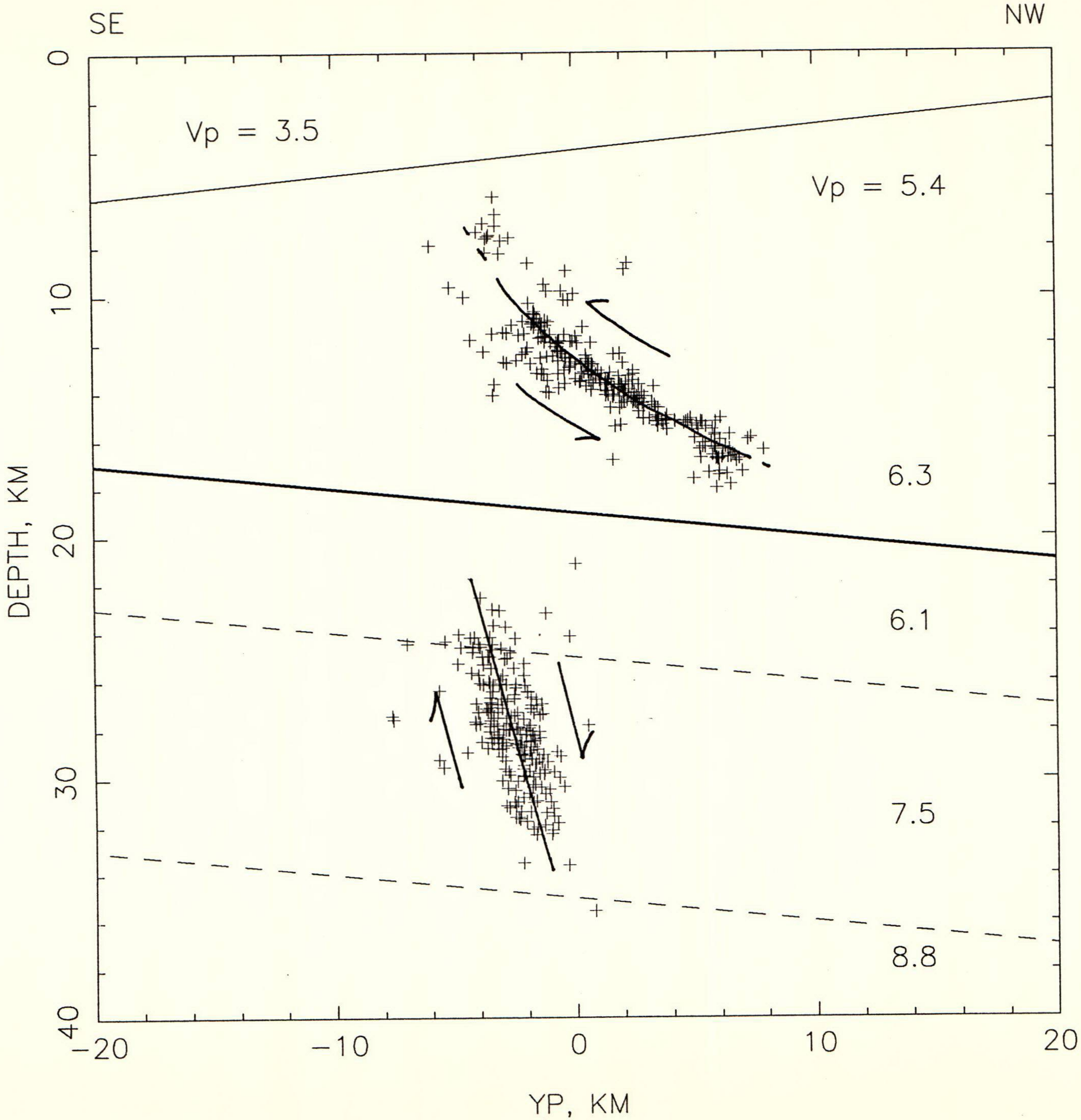

(14B)